A positivity-preserving Active Flux method for the Vlasov-Poisson system

Yanick Kiechle, Erik Chudzik, Christiane Helzel

Suggested Citation:
Kiechle, Y., Chudzik, E., & Helzel, C. (2024). A positivity-preserving Active Flux method for the Vlasov-Poisson system. Journal of Computational Physics, 524, Article 113693.
https://doi.org/10.1016/j.jcp.2024.113693

Journal of Computational Physics 524 (2025) 113693

Contents lists available at ScienceDirect

Journal of Computational Physics

journal homepage: www.elsevier.com/locate/jcp

A positivity-preserving Active Flux method for the Vlasov-Poisson system

Yanick Kiechle, Erik Chudzik, Christiane Helzel *

Faculty of Mathematics and Natural Sciences, Institute of Mathematics, Heinrich-Heine-University Düsseldorf, Germany

ARTICLE INFO

Keywords:
Active Flux
Positivity preservation
Flux limitation
Vlasov equation
Plasma physics

ABSTRACT

The Active Flux method is a finite volume method which uses point values as well as cell average values as degrees of freedom. The point values are evolved in time using the characteristic form of the equation while the conservative form of the equations is used to evolve cell average values. Here we present an Active Flux method for the $1 + 1$ dimensional Vlasov-Poisson system. The resulting scheme is third order accurate and uses a compact stencil in space and time. This leads to accurate approximations on relatively coarse grids, a desirable property for high dimensional kinetic equations.

To avoid negative values in the approximation of the Vlasov equation we introduce a new limiting approach for Active Flux methods that is motivated by positivity-preserving flux limiters.

1. Introduction

In this work we address the topic of flux limitation for Active Flux methods and present a positivity-preserving Active Flux method for the 1+1 dimensional Vlasov-Poisson system.

The Active Flux method is a finite volume method for hyperbolic conservation laws introduced by Eymann and Roe [19,20], which in its simplest form for one-dimensional linear advection is equivalent with van Leer's scheme V, presented in [43]. In the original papers, Active Flux methods have been proposed as fully discrete, truly multi-dimensional and third order accurate methods. These properties are achieved by using a compact stencil in space and time and a piecewise quadratic reconstruction. The numerical fluxes are computed with higher order accurate quadrature formulas, typically Simpson's rule. These quadrature rules require point values of the solution at the old time level (which are assumed to be known) and at later times (which need to be computed). These point values are evolved in time using truly multi-dimensional exact or approximative evolution operators. The use of point values in addition to cell average values distinguishes Active Flux methods from most other finite volume schemes. Recently, semi-discrete methods that use the same degrees of freedom have been proposed, see for example [1–3]. Our Active Flux method for the Vlasov-Poisson system however benefits from a fully discrete approach.

Two-dimensional Active Flux methods were first introduced on unstructured triangular grids by Eymann and Roe [20] and later studied on Cartesian grids [7,26]. For the Vlasov-Poisson problem the Cartesian grid version is most suitable and we therefore restrict our considerations to Cartesian grids. The dense and compact stencil provides accurate approximations even on coarse grids by following the more physical approach of using as little information as possible outside the true domain of dependence as pointed out by Roe [37]. The development of limiting techniques for Active Flux methods is currently an active research topic. Here we propose a positivity-preserving Active Flux method for multi-dimensional advective transport that is based on [45,47,28].

* Corresponding author.
E-mail address: christiane.helzel@hhu.de (C. Helzel).

https://doi.org/10.1016/j.jcp.2024.113693
Received 10 May 2024; Received in revised form 30 November 2024; Accepted 17 December 2024

Available online 20 December 2024

The Vlasov-Poisson system, see [22] for more details, describes the interaction of a collision-less plasma with an electrostatic force. The model might be considered as a simplification of the Vlasov-Maxwell system, a common model for astrophysical plasmas, see for example [4], which describes the interaction of a plasma with an electromagnetic field. The numerical simulation of the Vlasov-Maxwell as well as the Vlasov-Poisson system is challenging. In general the Vlasov equation is a kinetic equation in space and velocity phase space. Hence a six-dimensional time dependent partial differential equation for a density distribution function describing the plasma that is coupled to a lower dimensional equation, which only depends on space. Solutions of the Vlasov-Poisson system conserve infinitely many quantities over time. Some of these quantities are used as diagnostics for numerical schemes. Here we will construct a positivity-preserving, conservative method. Consequently, our method preserves the L^1-norm of the Vlasov solution up to machine precision.

In the last 50 years many different numerical methods have been developed for the Vlasov-Poisson system. A very prominent method is the Particle-In-Cell (PIC) method [27], where the distribution function is evolved using macro-particles. While this approach efficiently treats the high dimensionality, the method is less accurate in low-density regions.

Semi-Lagrangian methods, which are attractive for accuracy and stability reasons, have been studied intensively in particular by Sonnendrücker and collaborators [23,9,40,8,16]. This work also influenced the development of new discontinuous Galerkin methods [38,35,17] as well as WENO methods [34,44].

In higher dimensions, grid-based methods for the Vlasov equation typically relay on some form of splitting as pioneered by Cheng and Knorr [12].

Another interesting approach is given by spectral methods, which discretise the high dimensional Vlasov equation by a lower dimensional, i.e. only spatially dependent, system of moment equations. Recently, Filbet and Xiong [25] proposed a spectral method for the Vlasov-Poisson problem where the moments satisfy a system of hyperbolic partial differential equations. With their approach exact preservation of mass, momentum and energy is obtained, as those quantities are moments of the Vlasov equation and thus directly approximated.

Higher order accurate grid based methods require some form of limiting to avoid negative values of the density distribution function while accurately approximating the filamentation observed in plasma applications. This has previously been done by adapting limiting techniques from the Computational Fluid Dynamics community to different Vlasov solvers, including for example [24,38,35]. The limiting suggested for our Active Flux based Vlasov solver will also follow this path.

The Active Flux method introduced in this work has similarities with semi-Lagrangian methods. Similar to semi-Lagrangian methods we use characteristics to describe the evolution of the point values. For stability reasons, the Active Flux method requires the footpoint of the characteristic curve to be located in a neighbouring grid cell. While this leads to a stronger restriction of the time step it provides a scheme with a compact stencil in space and time. Banks and Hittinger [5] pointed out that local schemes are of particular interest when using parallel computing.

We believe that the Vlasov-Poisson system is an interesting model problem for the use of Active Flux methods. We obtain third order accurate approximations of the coupled Vlasov-Poisson problem by using a single solve of the Poisson problem and a single solve for the Vlasov problem per time step. Moreover, the limiting approach introduced in this paper does not degrade the accuracy of smooth solutions and should be of general interest also for other applications of the Active Flux method. The local stencil provides methods that are accurate even on coarse grids. Furthermore, the stencil should also simplify the use of this method in the context of interface coupling where different models might be solved in different parts of the computational domain. We plan to explore this aspect in forthcoming work.

The rest of this article is structured as follows: In Section 2, we begin with a short revision of Active Flux methods on two-dimensional Cartesian grids. In Section 3, we present an Active Flux method for advective transport in an externally imposed divergence-free, spatially and temporally varying velocity field and introduce a positivity-preserving flux limiter. As a more advanced problem we present the guiding-center model, where both an advected quantity as well as the divergence free velocity field are evolved in time. Finally, in Section 4 we describe our third order accurate positivity-preserving Active Flux method for the 1+1 dimensional Vlasov-Poisson system and present numerical solutions for classical problems.

Note that first work on the unlimited Active Flux method for Vlasov-Poisson was presented in the conference proceeding paper [29].

2. The two-dimensional Active Flux method

We consider the two-dimensional hyperbolic problem

$$\begin{aligned} \partial_t q + \partial_x f(q) + \partial_y g(q) &= 0 \qquad && x, y \in \mathbb{R}, t \in \mathbb{R}^+, \\ q(x, y, 0) &= q_0(x, y) && x, y \in \mathbb{R}, \end{aligned} \tag{1}$$

where $q : \mathbb{R}^2 \times \mathbb{R}^+ \to \mathbb{R}^m$ is a vector of $m \in \mathbb{N}$ conserved quantities and $f, g : \mathbb{R}^m \to \mathbb{R}^m$ are vector valued flux functions. We use a two-dimensional Cartesian grid with constant mesh widths Δx and Δy. A cell $C_{i,j}$ is given by $[x_{i-\frac{1}{2}}, x_{i+\frac{1}{2}}] \times [y_{j-\frac{1}{2}}, y_{j+\frac{1}{2}}]$, $i, j \in \mathbb{Z}$. Since Active Flux methods are finite volume methods, we calculate the cell average updates by

$$Q_{i,j}^{n+1} = Q_{i,j}^n - \frac{\Delta t}{\Delta x}\left(F_{i+\frac{1}{2},j} - F_{i-\frac{1}{2},j}\right) - \frac{\Delta t}{\Delta y}\left(G_{i,j+\frac{1}{2}} - G_{i,j-\frac{1}{2}}\right). \tag{2}$$

Here $Q^n_{i,j}$ denotes approximations to the cell average of the conserved quantities in cell $C_{i,j}$ at time t_n. $F_{i\pm\frac{1}{2},j}$ and $G_{i,j\pm\frac{1}{2}}$ are the numerical fluxes over the vertical respectively horizontal interfaces of $C_{i,j}$, i.e.

$$F_{i+\frac{1}{2},j} \approx \frac{1}{\Delta t \Delta y} \int_{t_n}^{t_{n+1}} \int_{y_{j-\frac{1}{2}}}^{y_{j+\frac{1}{2}}} f(q(x_{i+\frac{1}{2}}, y, t))\, dy\, dt, \tag{3}$$

$$G_{i,j+\frac{1}{2}} \approx \frac{1}{\Delta t \Delta x} \int_{t_n}^{t_{n+1}} \int_{x_{i-\frac{1}{2}}}^{x_{i+\frac{1}{2}}} g(q(x, y_{j+\frac{1}{2}}, t))\, dx\, dt. \tag{4}$$

As proposed by Eymann and Roe, we compute these numerical fluxes using Simpson's rule. In the two-dimensional case we obtain the formula

$$\begin{aligned} F_{i+\frac{1}{2},j} = \frac{1}{36}\Big(& f\left(Q^n_{i+\frac{1}{2},j-\frac{1}{2}}\right) + 4f\left(Q^n_{i+\frac{1}{2},j}\right) + f\left(Q^n_{i+\frac{1}{2},j+\frac{1}{2}}\right) \\ & + 4f\left(Q^{n+\frac{1}{2}}_{i+\frac{1}{2},j-\frac{1}{2}}\right) + 16f\left(Q^{n+\frac{1}{2}}_{i+\frac{1}{2},j}\right) + 4f\left(Q^{n+\frac{1}{2}}_{i+\frac{1}{2},j+\frac{1}{2}}\right) \\ & + f\left(Q^{n+1}_{i+\frac{1}{2},j-\frac{1}{2}}\right) + 4f\left(Q^{n+1}_{i+\frac{1}{2},j}\right) + f\left(Q^{n+1}_{i+\frac{1}{2},j+\frac{1}{2}}\right)\Big) \end{aligned} \tag{5}$$

and analogously for the numerical flux $G_{i,j+\frac{1}{2}}$. The values arising in the formulation of the numerical flux are quantities at times $t_n, t_{n+\frac{1}{2}}$ and t_{n+1}. The conserved quantities at time t_n are point values along the boundary of the cell $C_{i,j}$, namely on the midpoints of the edges $Q_{i+\frac{1}{2},j}$ and in corners $Q_{i+\frac{1}{2},j\pm\frac{1}{2}}$. These point values and the cell average are used to reconstruct a two-dimensional polynomial in each grid cell, which interpolates all eight point values and maintains the cell average. Using coordinate transformations, one can map the grid cell onto a reference cell $[-1,1]\times[-1,1]$. Locally in each cell, the mapped reconstructed polynomial is described by

$$q^{rec}(\xi,\eta) = c_{00} + c_{10}\xi + c_{01}\eta + c_{11}\xi\eta + c_{20}\xi^2 + c_{21}\xi^2\eta + x_{12}\xi\eta^2 + c_{02}\eta^2 + c_{22}\xi^2\eta^2, \tag{6}$$

with $c_{i,j} \in \mathbb{R}^m$, $i,j = 0,1,2$ and $(\xi,\eta) \in [-1,1]^2$. The reconstruction can be described using appropriate basis functions, see [7,26] for more details. We denote the reconstructed continuous piecewise quadratic function at time t_n by q^n. Furthermore, the piecewise quadratic polynomial in cell $C_{i,j}$ is denoted by $q^n_{i,j}$. In Active Flux methods the point values at times $t_{n+\frac{1}{2}}$ and t_{n+1} are of special interest. These values are unknown and need to be approximated separately. The calculation of the point values makes the method truly multi-dimensional. For simple linear partial differential equations such as advection or acoustics one can compute these point values using exact evolution operators, for other more complex problems, one needs to use approximations of the exact evolution operators, see [20,21,6,13,11,14]. Furthermore, the values of q at time t_{n+1} are of double importance as they serve as quadrature points in the flux computation and as interpolating data for the reconstruction at time t_{n+1}.

As a preparation of our Active Flux method for the Vlasov-Poisson problem we next consider advective transport and propose a new limiting strategy.

3. Advective transport in a divergence-free velocity field and a new positivity-preserving limiter

In this section we consider two-dimensional advective transport with a spatially and possibly temporally varying velocity field

$$\begin{aligned} \frac{\partial}{\partial t}q(x,y,t) + \frac{\partial}{\partial x}(a(x,y,t)q(x,y,t)) + \frac{\partial}{\partial y}(b(x,y,t)q(x,y,t)) = 0 \\ q(x,y,0) = q_0(x,y). \end{aligned} \tag{7}$$

If the velocity field is divergence-free, then (7) is equivalent to

$$\begin{aligned} \frac{\partial}{\partial t}q(x,y,t) + a(x,y,t)\frac{\partial}{\partial x}q(x,y,t) + b(x,y,t)\frac{\partial}{\partial y}q(x,y,t) = 0 \\ q(x,y,0) = q_0(x,y). \end{aligned} \tag{8}$$

In (8), which is sometimes called the colour equation, the variable q is transported such that its total derivative along a streamline is zero. Therefore, the exact solution is bound-preserving in the sense that for all later times the solution satisfies $q(x,y,t) \in [m,M]$ with $m := \min_{x,y} q_0(x,y)$, $M := \max_{x,y} q_0(x,y)$. For general velocity fields, which do not satisfy the divergence-free conditions, solutions of (7) are not necessarily bound-preserving. Zhang and Shu [45] pointed out that this discrepancy of the two models makes it difficult to construct perfectly bound-preserving methods by discretising the conservative form of the equation.

Fig. 1. Solution structure of LeVeque's test problem (7), (10), (11) computed with the Active Flux method on a grid with 200×200 cells.

3.1. Active Flux for advective transport

In our Active Flux method the evolution of the point values uses characteristic theory, i.e. for each point value we solve the ODE system

$$\begin{aligned} x'(t) &= a(x(t), y(t), t) \\ y'(t) &= b(x(t), y(t), t) \end{aligned} \tag{9}$$

with initial values $(x(0), y(0)) = (x_0, y_0)$, which correspond to the position of the considered point value, i.e. for the computation of point values $Q^{n+\frac{1}{2}}_{i+\frac{1}{2},j}$ and $Q^{n+1}_{i+\frac{1}{2},j}$ we use $(x_0, y_0) = (x_{i+\frac{1}{2}}, y_j)$. Here, we use the classical fourth order accurate Runge-Kutta method for the approximation of (9).

Note that we solve (9) with initial values (x_0, y_0) at time $t = 0$ backwards in time. The solutions at times $-\Delta t/2$ and $-\Delta t$ provide the location of the footpoint of the characteristics. We evaluate the Active Flux reconstruction at those points in order to compute the point values along the grid cell boundary at time $t_{n+\frac{1}{2}}$ and t_{n+1}, i.e. we compute for example

$$Q^{n+\frac{1}{2}}_{i+\frac{1}{2},j} = q^n \left(x_{i+\frac{1}{2}}(-\Delta t/2), y_j(-\Delta t/2) \right).$$

Finally, the numerical flux functions are obtained using (5) with

$$f(Q^{n+\frac{1}{2}}_{i+\frac{1}{2},j}) = a \left(x_{i+\frac{1}{2}}(-\Delta t/2), y_j(-\Delta t/2), t_{n+\frac{1}{2}} \right) Q^{n+\frac{1}{2}}_{i+\frac{1}{2},j}$$

and analogous expressions for the other values.

3.1.1. Numerical results for advective transport in an externally imposed spatially varying velocity field

To illustrate the performance of the Active Flux method for advective transport we consider a test problem proposed in [30], where advective transport takes place in a two-dimensional flow field of the form

$$a(x, y) = \sin^2(\pi x) \sin(2\pi y), \quad b(x, y) = -\sin^2(\pi y) \sin(2\pi x). \tag{10}$$

The computation is performed on the domain $[0, 1] \times [0, 1]$ using the initial values

$$q(x, y, 0) = \begin{cases} 1 & : \quad (x-1)^2 + (y-1)^2 < 0.8^2 \\ 0 & : \quad \text{otherwise.} \end{cases} \tag{11}$$

In Fig. 1 we show the solution structure at times $t = 0, 1, 2.5$ as a two-dimensional plot computed on a grid with 200×200 grid cells.

In Fig. 2 we show a slice of the solution along the line with $x = 0.5$. As expected, the unlimited Active Flux method shows some oscillations near the jump discontinuities but these oscillations are quite mild as also observed previously for third order Active Flux methods.

Different limited reconstructions have been proposed for the Active Flux method. While it is relatively simple to obtain a one-dimensional globally continuous bound-preserving reconstruction [26,6], the multi-dimensional situation is more challenging as can be seen in [2]. In [13] we proposed a piecewise quadratic bound-preserving reconstruction which is discontinuous across grid cell interfaces. The evolution of the point values described above does not rely on a continuous reconstruction. However, the point values at the old time level, which are used in Simpson's formula to compute the numerical fluxes, are no longer unique and instead need to be chosen in upwind direction as explained in [13]. In Fig. 3 we show numerical results for our test problem using the bound-

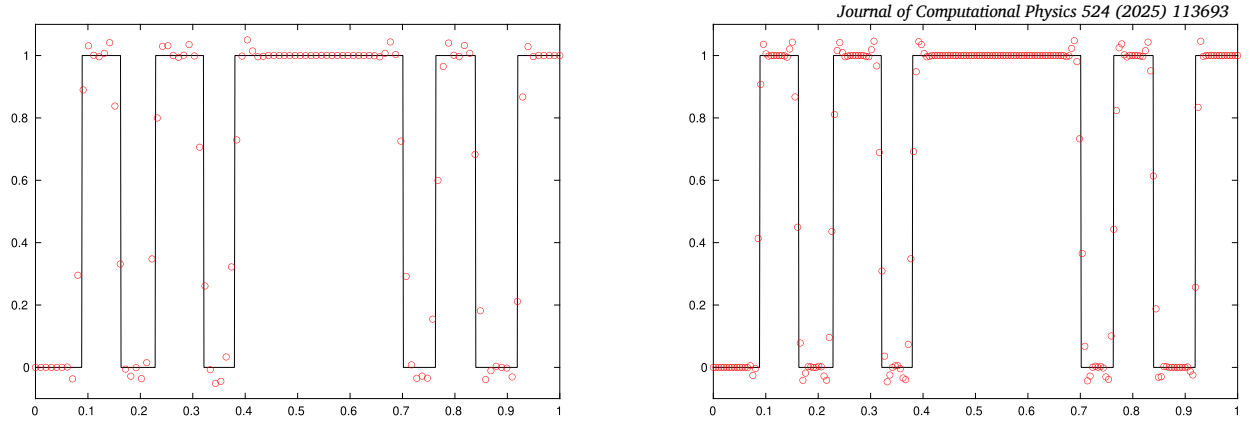

Fig. 2. Solution structure of LeVeque's test problem along the line $x = 0.5$ at time $t = 2.5$ computed using the Active Flux method with 100×100 (left) and 200×200 (right) grid cells.

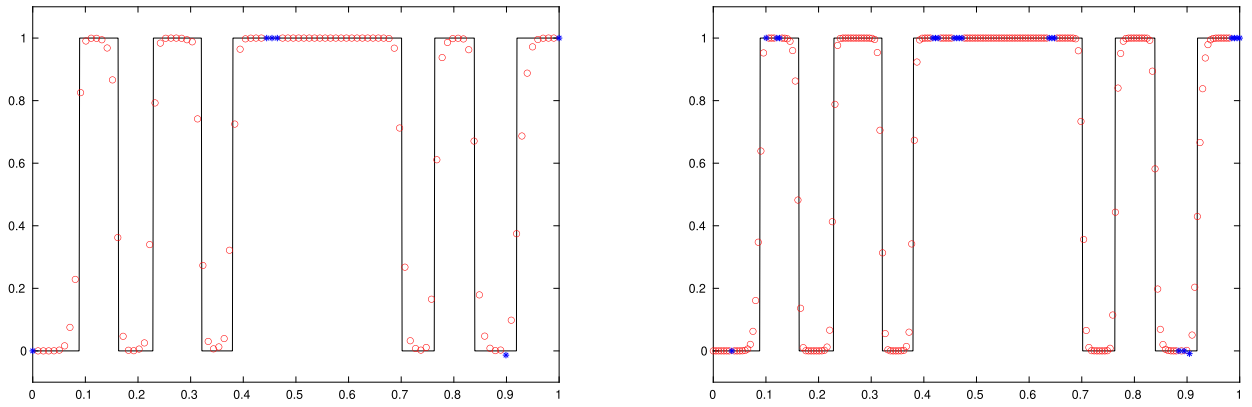

Fig. 3. Solution of LeVeque's test problem along the line $x = 0.5$ at time $t = 2.5$ using Active Flux with bound-preserving reconstruction. The computations used 100×100 (left) and 200×200 (right) grid cells. Cell average values outside the interval $[0, 1]$ are marked with blue stars; all other cell average values are marked as red circles. (For interpretation of the colours in the figure(s), the reader is referred to the web version of this article.)

preserving reconstruction. While the oscillations are clearly reduced, the numerical solution is not exactly bound-preserving. The reason for this behaviour is that Simpson's rule is not exact for piecewise quadratic functions.

We will now introduce a new flux limiter which leads to a positivity-preserving approximation of the cell average values. This is motivated by our main application, the approximation of the Vlasov-Poisson problem, where positivity of the distribution function is a desired property. For advective transport, this new limiting technique does not require the computation of a bound-preserving reconstruction. This speeds up the computation since we no longer need to compute local minima and maxima of the reconstructed function in each grid cell.

Applied to advective transport in a divergence-free, spatially varying velocity field, this will lead to a lower bound-preserving method.

3.2. Positivity-preserving flux limiter

Motivated by our main application, i.e. the approximation of the Vlasov-Poisson problem, we now introduce a flux limiter which preserves positivity of the solution. The flux limiting idea was first introduced by Zhang and Shu [46] for the approximation of the Euler equations of fluid mechanics. The limiting approach can be adapted to other conservation laws and we will here discuss its use for scalar two-dimensional conservation laws in the context of Active Flux methods.

Let us consider the two-dimensional initial value problem (1) with $m = 1$ and $f, g \in C^1(\mathbb{R})$ such that $q(x, y, t) \geq 0$ for all t.

The idea of the flux limiting approach is to replace the numerical fluxes $F_{i\pm\frac{1}{2},j}$, $G_{i,j\pm\frac{1}{2}}$ of the Active Flux method with limited fluxes, which are convex linear combinations of Active Flux and first order Lax-Friedrichs fluxes, i.e.

$$F^{lim}_{i-\frac{1}{2},j} := \gamma_{i-\frac{1}{2},j} F_{i-\frac{1}{2},j} + (1 - \gamma_{i-\frac{1}{2},j}) F^{LF}_{i-\frac{1}{2},j} \tag{12}$$

$$G^{lim}_{i,j-\frac{1}{2}} := \gamma_{i,j-\frac{1}{2}} G_{i,j-\frac{1}{2}} + (1 - \gamma_{i,j-\frac{1}{2}}) G^{LF}_{i,j-\frac{1}{2}} \tag{13}$$

choosing $\gamma_{i-\frac{1}{2},j}$ and $\gamma_{i,j-\frac{1}{2}}$ in a way that adds just enough numerical dissipation to obtain a positivity-preserving scheme.

The Lax-Friedrichs fluxes in the form used here are given by

$$F^{LF}_{i-\frac{1}{2},j} := \frac{1}{2}\left(f(Q^n_{i-1,j}) + f(Q^n_{i,j}) - a_x(Q^n_{i,j} - Q^n_{i-1,j})\right) \tag{14}$$

$$G^{LF}_{i,j-\frac{1}{2}} := \frac{1}{2}\left(g(Q^n_{i,j-1}) + g(Q^n_{i,j}) - a_y(Q^n_{i,j} - Q^n_{i,j-1})\right), \tag{15}$$

where a_x and a_y are the maximum signal speeds, i.e. $a_x = \max_i |f'(Q^n_{i,j})|$, $a_y = \max_j |g'(Q^n_{i,j})|$.

To derive the limiting coefficients, we rewrite the update of the cell averages (2) as a convex combination

$$\begin{aligned} Q^{n+1}_{i,j} = {} & \frac{\alpha_x}{2}\underbrace{\left(Q^n_{i,j} + 2\frac{\Delta t}{\alpha_x \Delta x} F_{i-\frac{1}{2},j}\right)}_{=:Q^-_i} + \frac{\alpha_x}{2}\underbrace{\left(Q^n_{i,j} - 2\frac{\Delta t}{\alpha_x \Delta x} F_{i+\frac{1}{2},j}\right)}_{=:Q^+_i} \\ & + \frac{\alpha_y}{2}\underbrace{\left(Q^n_{i,j} + 2\frac{\Delta t}{\alpha_y \Delta y} G_{i,j-\frac{1}{2}}\right)}_{=:Q^-_j} + \frac{\alpha_y}{2}\underbrace{\left(Q^n_{i,j} - 2\frac{\Delta t}{\alpha_y \Delta y} G_{i,j+\frac{1}{2}}\right)}_{=:Q^+_j} \end{aligned} \tag{16}$$

with $\alpha_x + \alpha_y = 1$ and $\alpha_x, \alpha_y > 0$. A sufficient condition for a positivity-preserving scheme is

$$Q^{\pm}_i \geq 0,\ Q^{\pm}_j \geq 0. \tag{17}$$

While the Lax-Friedrichs scheme is stable and positivity-preserving under the condition CFL $\leq \frac{1}{2}$, positivity of the quantities

$$Q^{LF,\pm}_i := Q^n_{i,j} \mp 2\frac{\Delta t}{\alpha_x \Delta x} F^{LF}_{i\pm\frac{1}{2},j}, \quad Q^{LF,\pm}_j := Q^n_{i,j} \mp 2\frac{\Delta t}{\alpha_y \Delta y} G^{LF}_{i,j\pm\frac{1}{2}} \tag{18}$$

in the special case $\alpha_x = \alpha_y = \frac{1}{2}$ is guaranteed only under the more restrictive condition CFL $\leq \frac{1}{4}$. Using these observations, we will now derive a limitation of the Active Flux flux function that ensures positivity.
Let $0 < \epsilon \ll 1$ and consider the case $Q^-_i < Q^{LF,-}_i$, which is equivalent to

$$F_{i-\frac{1}{2},j} < F^{LF}_{i-\frac{1}{2},j}. \tag{19}$$

We want to enforce the relation

$$\begin{aligned} Q^{lim,-}_i &:= Q^n_{i,j} + 2\frac{\Delta t}{\alpha_x \Delta x} F^{lim}_{i-\frac{1}{2},j} \\ &= Q^n_{i,j} + 2\frac{\Delta t}{\alpha_x \Delta x}\left(F^{LF}_{i-\frac{1}{2},j} + \gamma^-_{i-\frac{1}{2},j}\left(F_{i-\frac{1}{2},j} - F^{LF}_{i-\frac{1}{2},j}\right)\right) \\ &\geq \epsilon. \end{aligned} \tag{20}$$

Using (18) and (19) as well as $\frac{2\Delta t}{\alpha_x \Delta x}(F_{i-\frac{1}{2},j} - F^{LF}_{i-\frac{1}{2},j}) = Q^-_i - Q^{LF,-}_i$, it follows that (20) is satisfied under the condition

$$\gamma^-_{i-\frac{1}{2},j} \leq \frac{\epsilon - Q^{LF,-}_i}{Q^-_i - Q^{LF,-}_i}. \tag{21}$$

Furthermore, for $Q^+_i < Q^{LF,+}_i$, which is equivalent with $F_{i+\frac{1}{2},j} > F^{LF}_{i+\frac{1}{2},j}$, we insure

$$\begin{aligned} Q^{lim,+}_i &:= Q^n_{i,j} - 2\frac{\Delta t}{\alpha_x \Delta x} F^{lim}_{i+\frac{1}{2},j} \\ &= Q^n_{i,j} - 2\frac{\Delta t}{\alpha_x \Delta x}\left(F^{LF}_{i+\frac{1}{2},j} + \gamma^+_{i+\frac{1}{2},j}\left(F_{i+\frac{1}{2},j} - F^{LF}_{i+\frac{1}{2},j}\right)\right) \\ &\geq \epsilon \end{aligned}$$

if the inequality

$$\gamma^+_{i+\frac{1}{2},j} \leq \frac{\epsilon - Q^{LF,+}_i}{Q^+_i - Q^{LF,+}_i}$$

is satisfied. For the fluxes across horizontal grid cell interfaces we can analogously define and bound the quantities $Q^{lim,-}_j$ and $Q^{lim,+}_j$.

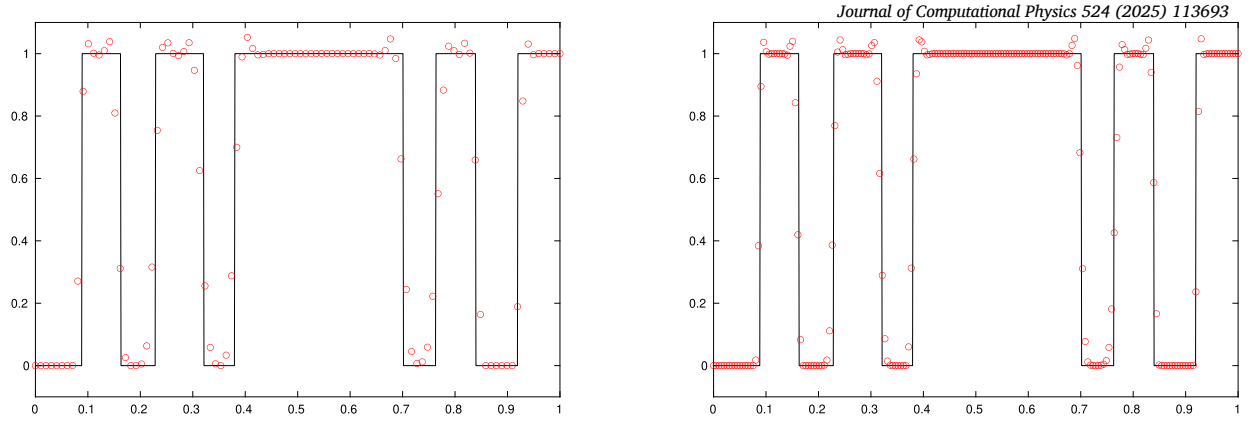

Fig. 4. Solution of LeVeque's test problem along the line $x = 0.5$ at time $t = 2.5$ using positivity-preserving flux limiter. The computations used 100×100 (left) and 200×200 (right) grid cells.

This motivates the definitions

$$\gamma^-_{i-\frac{1}{2},j} := \begin{cases} \frac{\epsilon - Q_i^{LF,-}}{Q_i^- - Q_i^{LF,-}} & : Q_i^- < \epsilon \\ 1 & : Q_i^- \geq \epsilon \end{cases}, \quad \gamma^+_{i-\frac{1}{2},j} := \begin{cases} \frac{\epsilon - Q_{i-1}^{LF,+}}{Q_{i-1}^+ - Q_{i-1}^{LF,+}} & : Q_{i-1}^+ < \epsilon \\ 1 & : Q_{i-1}^+ \geq \epsilon \end{cases} \tag{22}$$

and analogously

$$\gamma^-_{i,j-\frac{1}{2}} := \begin{cases} \frac{\epsilon - Q_j^{LF,-}}{Q_j^- - Q_j^{LF,-}} & : Q_j^- < \epsilon \\ 1 & : Q_j^- \geq \epsilon \end{cases}, \quad \gamma^+_{i,j-\frac{1}{2}} := \begin{cases} \frac{\epsilon - Q_{j-1}^{LF,+}}{Q_{j-1}^+ - Q_{j-1}^{LF,+}} & : Q_{j-1}^+ < \epsilon \\ 1 & : Q_{j-1}^+ \geq \epsilon \end{cases} \tag{23}$$

with $\epsilon := \max\{10^{-13}, \min q_0(x,y)\}$. Finally we define the unique limiting parameters at each grid cell interface

$$\gamma_{i-\frac{1}{2},j} := \min(\gamma^-_{i-\frac{1}{2},j}, \gamma^+_{i-\frac{1}{2},j}), \quad \gamma_{i,j-\frac{1}{2}} := \min(\gamma^-_{i,j-\frac{1}{2}}, \gamma^+_{i,j-\frac{1}{2}}). \tag{24}$$

Via construction, finite volume methods of the form (2) with limited fluxes (12) enforce positivity. In Fig. 4 we show slices of the solution structure along the line $x = 0.5$ using the positivity-preserving flux limiter. In addition we could of course also limit the point value updates using the bound-preserving reconstruction as outlined above. This would eliminate the oscillations near $q = 1$ but is not relevant for our main application.

For sufficiently smooth solutions, the flux limiter does not effect the order of accuracy of the Active Flux scheme. This was shown for general finite volume methods in [28]. In Section 4.4 we will present a numerical convergence study which confirms this result.

Remark 3.1. We observed that the computation of the limiting factor γ is sensitive to round off errors. Such inaccuracies might lead to values of γ outside the expected interval $[0, 1]$ and subsequently to approximations of the cell averages which are not positivity-preserving. To avoid such problems we replaced (24) in our implementation by

$$\gamma_{i-\frac{1}{2},j} := \max(\min(\gamma^-_{i-\frac{1}{2},j} - 10^{-16}, \gamma^+_{i-\frac{1}{2},j} - 10^{-16}, 1), 0),$$
$$\gamma_{i,j-\frac{1}{2}} := \max(\min(\gamma^-_{i,j-\frac{1}{2}} - 10^{-16}, \gamma^+_{i,j-\frac{1}{2}} - 10^{-16}, 1), 0).$$

Remark 3.2. In a recent publication, Abgrall et al. [3] proposed a *bound preserving* flux limiting for so-called point-average-moment polynomial-interpreted (PAMPA) schemes and presented very promising numerical results for one-dimensional hyperbolic problems including the Euler equations of gas dynamics. Third order accurate PAMPA methods use the same degrees of freedom as Active Flux methods, while the time evolution is performed using the method of lines approach. Their limiting approach is related to the limiting used here in the sense that the limited numerical flux is a linear combination of the high order flux and a low order Lax-Friedrichs flux. However, the approaches are not equivalent and the method from [3] is bound preserving, i.e. it preserves the upper and lower bound. Applied to our two-dimensional advective transport problem, their limited fluxes can be written in the form (12), (13) with

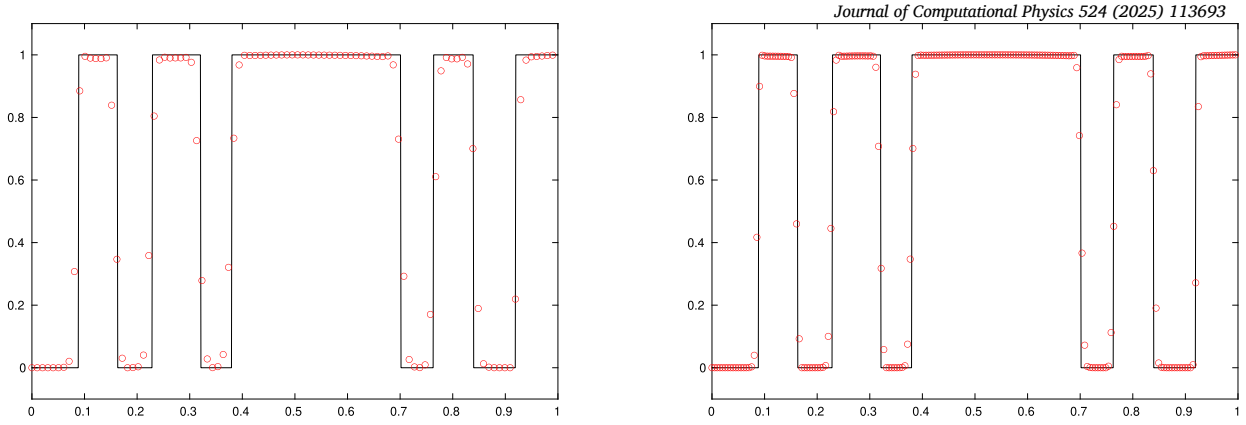

Fig. 5. Solution of LeVeque's test problem along the line $x = 0.5$ at time $t = 2.5$ using the bound-preserving flux limiter from [3] described in Remark 3.2. The computations used 100×100 (left) and 200×200 (right) grid cells.

$$\gamma_{i-\frac{1}{2},j} = \min\left(1, \frac{\alpha_{i-\frac{1}{2},j}}{|F^{AF}_{i-\frac{1}{2},j} - F^{LF}_{i-\frac{1}{2},j}|} \min\left(M_0 - u^*_{i-\frac{1}{2},j}, u^*_{i-\frac{1}{2},j} - m_0\right)\right),$$

$$u^*_{i-\frac{1}{2},j} = \frac{Q^n_{i,j} + Q^n_{i-1,j}}{2} - \frac{f(Q^n_{i,j}) - f(Q^n_{i-1,j})}{2\alpha_{i-\frac{1}{2},j}}.$$

Here, $\alpha_{i-\frac{1}{2},j}$ is an estimate of the local speed of propagation, which is also used in the computation of the Lax-Friedrichs flux, and M_0, m_0 are the upper and lower bounds of the solution that should be preserved by the numerical method. Analogously, the limiting-coefficients $\gamma_{i,j-\frac{1}{2}}$, for fluxes in the y-direction, can be computed. For our computation we used again a global estimate α_x instead of a local estimate $\alpha_{i-\frac{1}{2},j}$. While this leads to a more viscous Lax-Friedrichs flux it also leads to a larger value of $\gamma_{i-\frac{1}{2},j}$ and thus a larger portion of the high order flux is used. For our test problem this choice led to more accurate numerical results.

Furthermore, note that this bound preserving approach also requires a bound preserving approximation of point values to be used for the Active Flux flux computation. This can be obtained by an additional limiting process described in [3]. Here we simply replaced point value approximations outside the admissible domain $[0, 1]$ by point values obtained by tracing back the characteristics using a piecewise constant reconstruction. Numerical results applying this approach for LeVeque's test problem are shown in Fig. 5.

All of our computations presented in the reminder of the paper used our positivity-preserving approach as we never observed unphysical approximations of the density distribution function larger than one for our main application, i.e. the approximation of the Vlasov-Poisson problem.

3.3. Simulations of the guiding-center model

Now we consider advective transport in a coupled problem where the density as well as the velocity field are evolved in time. The coupled system has the form

$$\partial_t \rho + E^\perp \cdot \nabla \rho = 0, \tag{25}$$

$$-\Delta \Phi = \rho, \quad E = -\nabla \Phi. \tag{26}$$

This model has been studied in [18,16,41,31] to describe the evolution of a highly magnetized plasma in the poloidal plane of a tokamak. Previous authors pointed out that it is difficult to apply splitting strategies due to the multi-dimensional structure of the velocity field. This makes it a good test problem for our two-dimensional Active flux method.

The velocity field $E^\perp = (E_y(x, y), -E_x(x, y))$ is computed during each time step by solving a Poisson problem on a mesh of size $\Delta x/2$, $\Delta y/2$, i.e. we compute Φ at all point value degrees of freedom as well as in the center of the grid cells using known point values of ρ from the previous time t_n. We approximate the Poisson problem by using the 5-point stencil for the Laplace operator together with a multi-grid solver. Finite difference approximations of $\nabla\Phi$ provide the velocity field at time t_n at all point value degrees of freedom. In a predictor step we use these velocity components in order to compute point values of ρ at the intermediate time $t_{n+\frac{1}{2}}$ and the new time level t_{n+1}. Then we use these point values of ρ to compute the velocity field at $t_{n+\frac{1}{2}}$ and t_{n+1} by solving again two Poisson problems but now using the updated point values of ρ. In a corrector step, we use the updated velocity fields to compute new point values of ρ at $t_{n+\frac{1}{2}}$ and t_{n+1}. Finally, the cell averages at time t_{n+1} are computed using the finite volume approach outlined in (2)-(5). Positivity-preserving limiting has been applied to avoid negative cell average values of density.

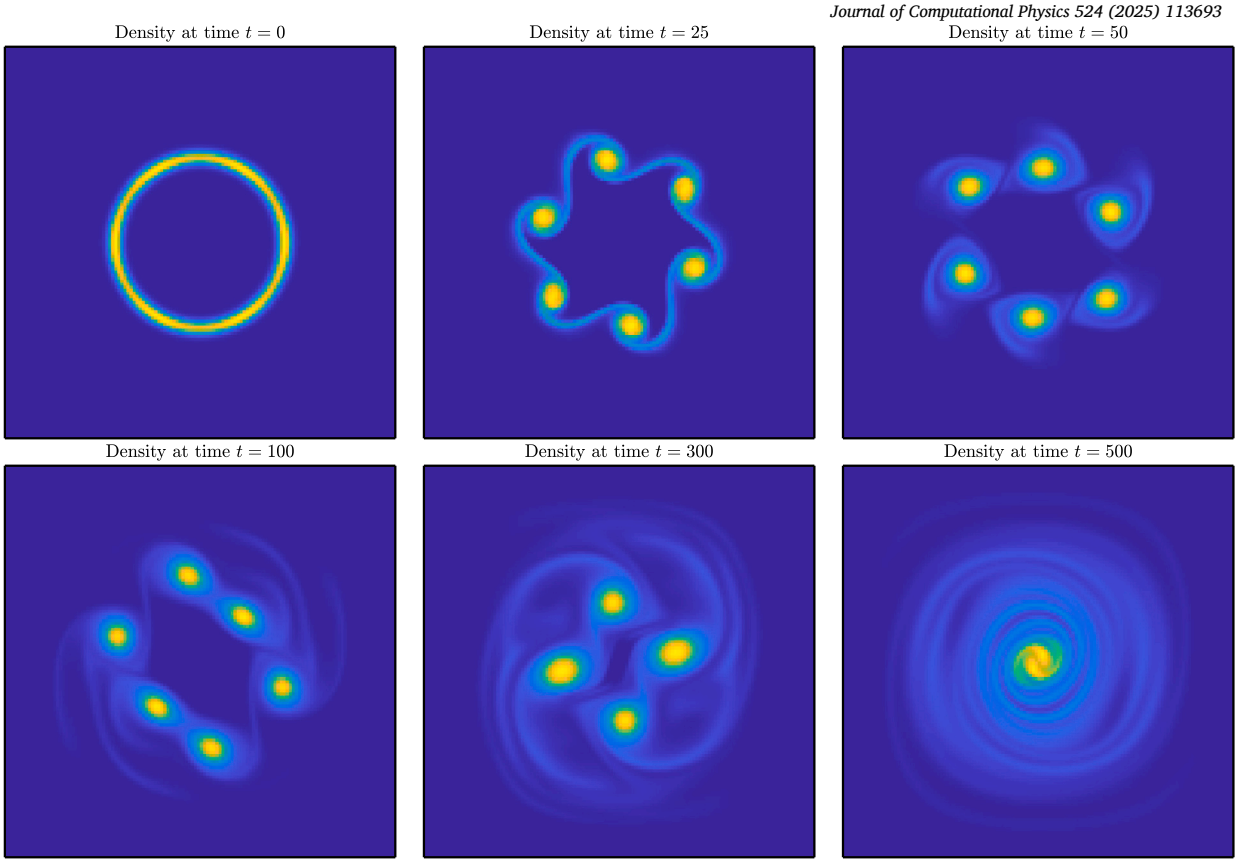

Fig. 6. Numerical solution of the guiding center model computed on a grid with 128×128 cells at different times.

To test our method we consider the diocotron instability studied in [15,31]. The initial data is given by

$$\rho_0(x,y) = \begin{cases} (1 + \varepsilon \cos(\ell\theta)) \exp(-4(r-6.5)^2), & \text{if } r^- \le \sqrt{x^2+y^2} \le r^+ \\ 0 & \text{otherwise.} \end{cases} \tag{27}$$

Here, we set $\theta = \operatorname{atan2}(y,x), r^- = 5, r^+ = 8, \ell = 6, \varepsilon = 0.1$. The computational domain is $[-15,15] \times [-15,15]$. Boundary values of Φ and ρ are set to zero. In Fig. 6 we present numerical results at different times computed ony a grid with 128×128 cells. We observe the formation of vortices which subsequently merge.

4. An Active Flux method for the Vlasov-Poisson system

We consider the single species 1+1-dimensional Vlasov-Poisson system

$$\partial_t f + v\partial_x f + E\partial_v f = 0 \tag{28}$$

$$\partial_{xx}\phi = \rho - \rho_0 \tag{29}$$

$$E = \partial_x \phi \tag{30}$$

on the domain $\Omega_x \times \Omega_v$ with periodic boundary conditions in x. Here,

$$\rho(x,t) := \int_{\Omega_v} f(x,v,t)\,dv, \quad \rho_0 := \frac{1}{|\Omega_x|}\int_{\Omega_x} \rho(x,t)\,dx \tag{31}$$

are the charge and background charge densities, respectively. The scalar quantity $f = f(x,v,t)$ is a distribution function. It describes the probability that at time t a plasma particle with velocity v is located at the position x. $E = E(x,t)$ is the electric field, which is computed from an electrostatic equation. Details on the derivation of the Vlasov-Poisson system from the Vlasov-Maxwell equations can be found in [38].

Analytical solutions of the Vlasov-Poisson system satisfy infinitely many conservation laws that can be used as diagnostics for numerical schemes. Here, we will in particular consider the following quantities:

- L^p-Norm:

$$\frac{\partial}{\partial t}\left(\int_{\Omega_x}\int_{\Omega_v} |f(x,v,t)|^p \, dv\, dx\right)^{\frac{1}{p}} = 0$$

- Total Energy:

$$\begin{aligned}\frac{\partial}{\partial t}\mathcal{E}(t) &= \frac{\partial}{\partial t}\mathcal{E}_e(t) + \frac{\partial}{\partial t}\mathcal{E}_k(t)\\ &= \frac{\partial}{\partial t}\frac{1}{2}\int_{\Omega_x} |E(x,t)|^2\, dx + \frac{\partial}{\partial t}\frac{1}{2}\int_{\Omega_x}\int_{\Omega_v} v^2 f(x,v,t)\, dv\, dx = 0\end{aligned}$$

  $\mathcal{E}_e$ being the electric or potential energy and $\mathcal{E}_k$ being the kinetic energy
- Entropy:

$$\frac{\partial}{\partial t}\left(-\int_{\Omega_x}\int_{\Omega_v} f(x,v,t)\log(f(x,v,t))\, dv\, dx\right) = 0$$

We will now propose a positivity-preserving, third order accurate Active Flux method. Third order accuracy is achieved in a truly multi dimensional way without the use of operator splitting techniques. The availability of additional point values enables us to construct this method efficiently. We begin in Section 4.1 by discussing an unlimited Active Flux method for the Vlasov-Poisson system, which will be extended in 4.3 to a positivity-preserving method by applying the limiting strategy from 3.2. In Section 4.2, we briefly discuss the approximation of the electric field. One advantage of the proposed Active Flux method is that it requires only one Poisson and one Vlasov step per time step.

4.1. The numerical method

We use a Cartesian grid for the (x,v)-space which discretises the domain $\Omega_x \times \Omega_v$ with cells $C_{i,j} = [x_{i-\frac{1}{2}}, x_{i+\frac{1}{2}}] \times [v_{j-\frac{1}{2}}, v_{j+\frac{1}{2}}]$ of constant mesh widths $\Delta x = x_{i+\frac{1}{2}} - x_{i-\frac{1}{2}}$ and $\Delta v = v_{j+\frac{1}{2}} - v_{j-\frac{1}{2}}$. Since $\nabla_{(x,v)} \cdot \begin{pmatrix} v \\ E(x,t) \end{pmatrix} = 0$, we can reformulate the system (28) - (30) with flux functions $h(f) = vf(x,v,t)$ and $g(f) = E(x,t)f(x,v,t)$ and obtain the compact notation

$$\begin{aligned}\partial_t f + \partial_x h(f) + \partial_v g(f) &= 0,\\ \partial_{xx}\phi &= \rho - \rho_0,\\ E &= \partial_x \phi.\end{aligned}$$

Note that in this subsection the conserved quantity is f and therefore the cell average in cell $C_{i,j}$ will be denoted by $F^n_{i,j}$ and the point values along the boundary are $F^n_{i\pm\frac{1}{2},j\pm\frac{1}{2}}$, $F_{i\pm\frac{1}{2},j}$ and $F_{i,j\pm\frac{1}{2}}$. An illustration of the configuration of the degrees of freedom in one cell is given in Fig. 7.

For now, we concentrate on the update of the kinetic equation. In classical Active Flux fashion, we compute the numerical flux over a vertical edge $x_{i+\frac{1}{2}} \times [v_{j-\frac{1}{2}}, v_{j+\frac{1}{2}}]$ of the cell $C_{i,j}$, i.e.

$$H_{i+\frac{1}{2},j} \approx \frac{1}{\Delta t \Delta v}\int_{t_n}^{t_{n+1}}\int_{v_{j-\frac{1}{2}}}^{v_{j+\frac{1}{2}}} h(f(x_{i+\frac{1}{2}}, v, t))\, dv\, dt$$

as well as the flux over the horizontal edge $[x_{i-\frac{1}{2}}, x_{i+\frac{1}{2}}] \times v_{j+\frac{1}{2}}$ of $C_{i,j}$, i.e.

$$G_{i,j+\frac{1}{2}} \approx \frac{1}{\Delta t \Delta x}\int_{t_n}^{t_{n+1}}\int_{x_{i-\frac{1}{2}}}^{x_{i+\frac{1}{2}}} g(f(x, v_{j+\frac{1}{2}}, t))\, dx\, dt$$

using two-dimensional Simpson's rule. We obtain

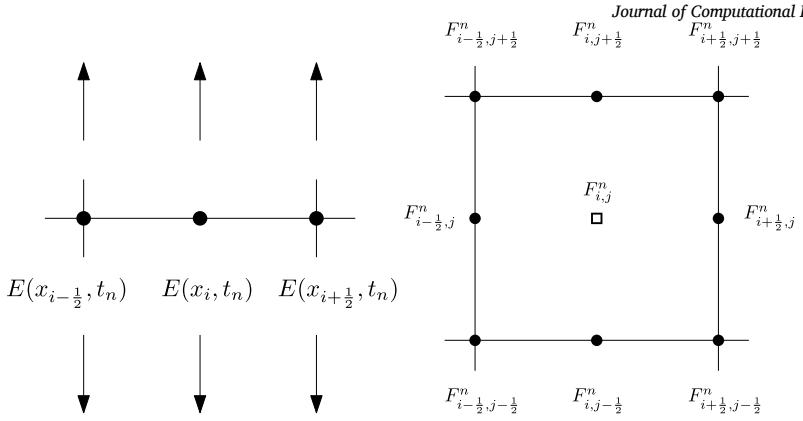

Fig. 7. Left: One-dimensional spatial grid cell of the electric field. The arrows are to illustrate the integration over the velocity space to obtain ρ. Right:Configuration of degrees of freedom in cell $C_{i,j}$.

$$\begin{aligned} H_{i+\frac{1}{2},j} = \frac{1}{36}\Big(& v_{j-\frac{1}{2}} F^n_{i+\frac{1}{2},j-\frac{1}{2}} + 4v_j F^n_{i+\frac{1}{2},j} + v_{j+\frac{1}{2}} F^n_{i+\frac{1}{2},j+\frac{1}{2}} \\ & + 4v_{j-\frac{1}{2}} F^{n+\frac{1}{2}}_{i+\frac{1}{2},j-\frac{1}{2}} + 16v_j F^{n+\frac{1}{2}}_{i+\frac{1}{2},j} + 4v_{j+\frac{1}{2}} F^{n+\frac{1}{2}}_{i+\frac{1}{2},j+\frac{1}{2}} \\ & + v_{j-\frac{1}{2}} F^{n+1}_{i+\frac{1}{2},j-\frac{1}{2}} + 4v_j F^{n+1}_{i+\frac{1}{2},j} + v_{j+\frac{1}{2}} F^{n+1}_{i+\frac{1}{2},j+\frac{1}{2}} \Big) \end{aligned} \tag{32}$$

and

$$\begin{aligned} G_{i,j+\frac{1}{2}} = \frac{1}{36}\Big(& E^n_{i-\frac{1}{2}} F^n_{i-\frac{1}{2},j+\frac{1}{2}} + 4E^n_i F^n_{i,j+\frac{1}{2}} + E^n_{i+\frac{1}{2}} F^n_{i+\frac{1}{2},j+\frac{1}{2}} \\ & + 4E^{n+\frac{1}{2}}_{i-\frac{1}{2}} F^{n+\frac{1}{2}}_{i-\frac{1}{2},j+\frac{1}{2}} + 16E^{n+\frac{1}{2}}_i F^{n+\frac{1}{2}}_{i,j+\frac{1}{2}} + 4E^{n+\frac{1}{2}}_{i+\frac{1}{2}} F^{n+\frac{1}{2}}_{i+\frac{1}{2},j+\frac{1}{2}} \\ & + E^{n+1}_{i-\frac{1}{2}} F^{n+1}_{i-\frac{1}{2},j+\frac{1}{2}} + 4E^{n+1}_i F^{n+1}_{i,j+\frac{1}{2}} + E^{n+1}_{i+\frac{1}{2}} F^{n+1}_{i+\frac{1}{2},j+\frac{1}{2}} \Big). \end{aligned} \tag{33}$$

Here $E_i^{n+\frac{\tau}{\Delta t}}$ denotes the approximations of the electric field $E(x_i, t_n+\tau)$ for $\tau \in \{0, \frac{\Delta t}{2}, \Delta t\}$. As Active Flux is a third order accurate fully discrete finite volume method, we need to ensure that the numerical fluxes are computed accurately enough. In (32) the v values are simply discretisations of the velocity space and thus known exactly. The point values of f at the previous, intermediate and new time level are computed with third order accuracy using the method of characteristics as explained in more detail below. The computation of (33) requires in addition to the point values of f also point values of the electric field. The approximation of the electric field at current time t_n is described in Section 4.2. Therefore, let us assume we have at least third order accurate approximations of the electric field on each interface as well as in the middle of the one dimensional cell $[x_{i-\frac{1}{2}}, x_{i+\frac{1}{2}}]$, i.e. $E^n_{i-\frac{1}{2}} \approx E(x_{i-\frac{1}{2}}, t_n)$, $E^n_i \approx E(x_i, t_n)$ for all $i = \frac{1}{2}, \dots, N_x + \frac{1}{2}$. To obtain approximations of the electric field at $t = t_{n+\frac{1}{2}}$ and $t = t_{n+1}$, we need a representation of the electric field as a function of time. This can be obtained by a Taylor series expansion as proposed in [38]. Consider

$$E(x, t_n + \tau) = E(x, t_n) + \tau E_t(x, t_n) + \frac{1}{2!}\tau^2 E_{tt}(x, t_n) + \mathcal{O}(\tau^3) \tag{34}$$

for $\tau \in [0, \Delta t]$. To obtain third order accuracy of $E(x, t_n + \tau)$ in time, a second order accurate approximation of E_t and a first order accurate approximation of E_{tt} are sufficient since

$$E(x, t_n + \tau) = \underbrace{E(x, t_n)}_{=\mathcal{O}(\tau^3)} + \tau \underbrace{E_t(x, t_n)}_{=\mathcal{O}(\tau^2)} + \frac{1}{2!}\tau^2 \underbrace{E_{tt}(x, t_n)}_{=\mathcal{O}(\tau)} + \mathcal{O}(\tau^3) = \mathcal{O}(\tau^3).$$

The time derivatives of the electric field can be calculated by moments of the Vlasov equation (28):

$$E_t(x, t) = -\rho u(x, t), \quad E_{tt}(x, t) = \partial_x \mathbb{E}(x, t_n) - \rho(x, t_n) E(x, t_n), \tag{35}$$

where $\rho u(x, t) := \int_{\Omega_v} v f \, dv$ and $\mathbb{E} := \int_{\Omega_v} v^2 f \, dv$. See [38] for a more detailed derivation of these equations. Using the degrees of freedom of the Active Flux method, these integrals can be approximated using Simpson's rule. We get

$$\mathbb{E}^n_{i-\frac{1}{2}} = \frac{\Delta v}{6}\sum_{j=1}^{N_v}(v^2_{j-\frac{1}{2}}F^n_{i-\frac{1}{2},j-\frac{1}{2}} + 4v_j^2 F^n_{i-\frac{1}{2},j} + v^2_{j+\frac{1}{2}}F^n_{i-\frac{1}{2},j+\frac{1}{2}})$$
$$\mathbb{E}^n_i = \frac{\Delta v}{6}\sum_{j=1}^{N_v}\Big(v^2_{j-\frac{1}{2}}F^n_{i,j-\frac{1}{2}} + v^2_{j+\frac{1}{2}}F^n_{i,j+\frac{1}{2}} + 4v_j^2\frac{1}{16}\big(36F^n_{i,j} - 4(F^n_{i,j-\frac{1}{2}} + F^n_{i+\frac{1}{2},j} + F^n_{i,j+\frac{1}{2}} + F^n_{i-\frac{1}{2},j}) - (F^n_{i-\frac{1}{2},j-\frac{1}{2}} + F^n_{i+\frac{1}{2},j-\frac{1}{2}} + F^n_{i+\frac{1}{2},j+\frac{1}{2}} + F^n_{i-\frac{1}{2},j+\frac{1}{2}})\big)\Big) \tag{36}$$

for $i = \frac{1}{2},\dots,N_x+\frac{1}{2}$. For the approximation of $\mathbb{E}_{i-\frac{1}{2}}$ we can directly use the point value degrees of freedom. The computation of $\mathbb{E}_i$ requires point values of f at the midpoints of a grid cell. These point values need to be computed from the Active Flux reconstruction. With the approximation $\mathbb{E}^n_i$ we compute numerically, using finite differences, the partial derivative of $\mathbb{E}(x,t_n)$ at the points x_i for $i = \frac{1}{2},\dots,N_x+\frac{1}{2}$. We use the following fourth order finite difference scheme

$$\partial_x\mathbb{E}(x_i,t_n) \approx \frac{\mathbb{E}^n_{i-\frac{3}{2}} - 8\mathbb{E}^n_{i-\frac{1}{2}} + 8\mathbb{E}^n_{i+\frac{1}{2}} - \mathbb{E}^n_{i+\frac{3}{2}}}{12\frac{\Delta x}{2}} \tag{37}$$

for all $i = \frac{1}{2},\dots,N_x+\frac{1}{2}$. Similar to the calculations in (36) one computes approximations of ρ and ρu. Once we have computed

$$\rho^n_i \approx \rho(x_i,t_n), \quad (\rho u)^n_i \approx \rho u(x_i,t_n), \quad \text{and} \quad \mathbb{E}^n_{i,x} \approx \partial_x\mathbb{E}(x_i,t_n) \tag{38}$$

for $i = \frac{1}{2},1,\dots,N_x+\frac{1}{2}$, we obtain

$$E^n_{i,t} = -(\rho u)^n_i \quad \text{and} \quad E^n_{i,tt} = \mathbb{E}^n_{i,x} - \rho^n_i E^n_i, \tag{39}$$

and finally

$$E^{n+\frac{\tau}{\Delta t}}_i = E^n_i + \tau E^n_{i,t} + \frac{\tau^2}{2!}E^n_{i,tt} \tag{40}$$

for $i = \frac{1}{2},1,\dots,N_x+\frac{1}{2}$ and $\tau \in [0,\Delta t]$.
With this procedure we have approximations of the electric field at the intermediate and new time level with sufficient accuracy. Thus we can compute the values of the electric field needed to compute the numerical fluxes (33).

To obtain a complete description of the numerical fluxes $G_{i,j+\frac{1}{2}}$ and $H_{i+\frac{1}{2},j}$, we still need to compute the point values of f at the intermediate and new time level. Similar to the method described in Section 3.1, we consider the system of ODEs associated with the characteristics of the equation (28), i.e.

$$\begin{aligned} x'(t) &= v(t), \\ v'(t) &= E(x(t),t), \end{aligned} \tag{41}$$

to develop a truly multi-dimensional method. We solve the ODE backwards in time for a half or full time step with the classical fourth order accurate Runge-Kutta method.

Note that there is an additional difficulty, which was not present in the test problem of Section 3.1. In order to numerically solve an initial values problem for the ODE (41), we need values of the electric field as a function of space and time. Via (40) we have expressed the electric field as a function of time at discrete points only. If we restrict the time step such that

$$\text{CFL} := \max\left(\frac{\max_j|v_j|\Delta t}{\Delta x}, \frac{\max_i|E(x_i,t)|\Delta t}{\Delta v}\right) \le 1,$$

we need to evaluate the electric field within the grid cell to the left or right of the considered interface only. Therefore we can easily use Lagrangian interpolation to obtain a representation of the electric field that can be evaluated at any point of interest. For example, we may interpolate locally in the one dimensional cell $[x_{i-\frac{1}{2}}, x_{i+\frac{1}{2}}]$

$$\left(x_{i-\frac{1}{2}}, E^{n+\tau}_{i-\frac{1}{2}}\right), \left(x_i, E^{n+\tau}_i\right), \left(x_{i+\frac{1}{2}}, E^{n+\tau}_{i+\frac{1}{2}}\right)$$

and get

$$E(x^*,t_n+\tau) = \sum_{k\in\{i-\frac{1}{2},i,i+\frac{1}{2}\}} E^{n+\tau}_k L_k(x^*)$$

for any $x^* \in [x_{i-\frac{1}{2}}, x_{i+\frac{1}{2}}]$, where L_k are the Lagrangian basis polynomials. Once the footpoints of the characteristic curves are computed, we obtain the desired point values by evaluating the piecewise quadratic Active Flux reconstruction of f. An illustration is given in Fig. 8.

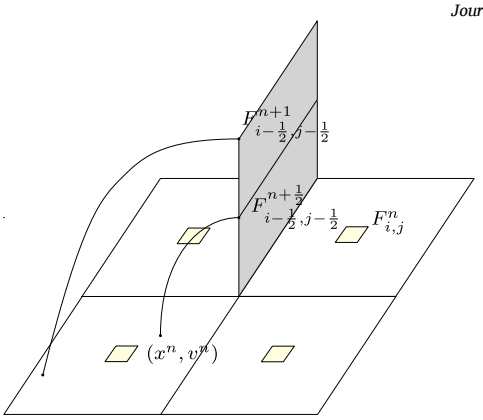

Fig. 8. Illustration of the evolution of point values in Vlasov-Poisson.

After all quantities of the numerical fluxes are calculated, the new cell averages are given by the finite volume method

$$F^{n+1}_{i,j} = F^n_{i,j} - \frac{\Delta t}{\Delta x}\left(H_{i+\frac{1}{2},j} - H_{i-\frac{1}{2},j}\right) - \frac{\Delta t}{\Delta v}\left(G_{i,j+\frac{1}{2}} - G_{i,j-\frac{1}{2}}\right).$$

4.2. The Poisson problem

In this subsection we describe the approximation of the electric field at current time t_n. We saw in the calculation of the numerical flux $G_{i,j+\frac{1}{2}}$ that the electric field needs to be calculated at the grid cell interfaces and midpoints, as one can see in Fig. 7. Subsequently, we approximate the electric field on a one-dimensional grid which discretises the interval $\Omega_x := (a_x, b_x)$ with constant mesh width $\frac{\Delta x}{2}$. The computation of the electric field is performed using a higher order finite difference scheme. To obtain a unique solution to the Poisson problem with periodic boundary condition, we solve

$$\partial_{xx}\phi(x,t) = \rho(x,t) - \rho_0 \tag{42}$$

$$\phi(a_x,t) = \phi(b_x,t) = 0, \tag{43}$$

numerically with ρ and ρ_0 being computed via Simpson's rule as described above. We use the following fourth order accurate finite difference scheme for the approximation of (42)

$$\partial_{xx}\phi(x,t_n) \approx \frac{-\phi^n_{i-\frac{3}{2}} + 16\phi^n_{i-\frac{1}{2}} - 30\phi^n_i + 16\phi^n_{i+\frac{1}{2}} - \phi^n_{i+\frac{3}{2}}}{12\frac{\Delta x}{2}}. \tag{44}$$

From the solution $\phi^n_i \approx \phi(x_i, t_n)$ for $i = \frac{1}{2}, \dots, N_x + \frac{1}{2}$ we compute the electric field using the same finite difference method for the first derivative as in (37).

4.3. Limiting

Since our solution f is a distribution function and thus non-negative, one aims to develop a method that is positivity-preserving. We therefore apply the positivity-preserving flux limiter described in Section 3.2. This limiting procedure uses Lax-Friedrichs numerical flux functions which for the Vlasov-Poisson system are given by

$$H^{LF}_{i-\frac{1}{2},j} = \frac{1}{2}\left(v_j F^n_{i-1,j} + v_j F^n_{i,j} - \max_j(|v_j|)\left(F^n_{i,j} - F^n_{i-1,j}\right)\right)$$

and

$$G^{LF}_{i,j-\frac{1}{2}} = \frac{1}{2}\left(E^n_i F^n_{i,j-1} + E^n_i F^n_{i,j} - \max_i(|E^n_i|)\left(F^n_{i,j} - F^n_{i,j-1}\right)\right).$$

In Algorithm 1 we summarise all the steps required to perform one time step of the Active Flux method for the Vlasov-Poisson problem.

4.4. Numerical results for the Vlasov-Poisson system

Finally, we present numerical simulations of the Vlasov-Poisson system for several classical test problems. In addition to approximations of the density distribution function f we discuss the approximation of diagnostic quantities mentioned in Section 4. To

Algorithm 1 One time step of the Active Flux method for Vlasov-Poisson.

Solve **Poisson problem** and calculate $E(x,t_n)$ as described in Section 4.2.
Compute $E_t(x,t_n)$, $E_{tt}(x,t_n)$ and $E(x,t_n+\tau)$ for $\tau \in \{\frac{\Delta t}{4}, \frac{\Delta t}{2}, \Delta t\}$ using (39), (40).

for $i = 1,2,\dots,N_x$ **do**
  for $j = 1,2,\dots,N_v$ **do**
    Evolve **point values** in each cell $C_{i,j}$ for a full and half time-step by solving (41) backwards in time and evaluating the Active Flux reconstruction of the density distribution function f along the grid cell boundary at times $t_{n+\frac{1}{2}}$ and t_{n+1}.
    Compute **limited numerical fluxes** using (32), (33) and the limiter from Sections 3.2 and 4.3.
    Calculate new **cell averages** $F_{i,j}^{n+1}$ using finite volume approach.
  end for
end for

Table 1
Convergence study for the unlimited and limited Active Flux method for the two-stream instability problem at time $t = 1$.

Grid	NoLim		PosPres	
	L^1-Error	EOC	L^1-Error	EOC
32^2	3.1813×10^{-2}	—	3.3272×10^{-2}	—
64^2	4.7389×10^{-3}	2.7476	4.9808×10^{-3}	2.7398
128^2	6.3991×10^{-4}	2.8886	6.7479×10^{-4}	2.8841
256^2	8.2742×10^{-5}	2.9480	8.7326×10^{-5}	2.9461
512^2	1.0538×10^{-5}	2.9730	1.1128×10^{-5}	2.9722

investigate how well these quantities are preserved by the numerical method, we show the deviations of the quantities from their initial value as a function of time, normalised by the initial value.

By construction, our method preserves the L^1-norm of the density distribution function f up to machine precision. Therefore, we do not present this quantity.

4.4.1. The two-stream instability

First, we consider the two-stream instability problem for the Vlasov-Poisson system. We use the same initial values as in [38], i.e.

$$f(x,v,t=0) = \frac{v^2}{\sqrt{8\pi}} \left(2 - \cos\left(\frac{x}{2}\right)\right) e^{\frac{-v^2}{2}} \tag{45}$$

and impose double periodic boundary conditions on the domain $(-2\pi, 2\pi) \times (-2\pi, 2\pi)$. Initially, the solution consists of two beams propagating in opposite direction. This configuration is unstable and leads to an increase of the electric energy. At later times nonlinear effects dominate and the electric energy remains roughly constant while a filamentation of the vortex structure can be observed. In Fig. 9 we present results for the positivity-preserving method on grids with 64×64, 128×128, 256×256 and 512×512 cells at times $t = 15, 30, 45$. Additionally, we show vertical cross-sections at $x = 0$ of the corresponding solutions in Fig. 10. In these images, the solid line shows the limited positivity-preserving solution whereas the red crosses represent values of the unlimited solution. ClearIy, one can see on these images the impact of the flux limitation strategy. Negative values are suppressed but otherwise the solution structure is not disturbed. Note that all of our plots only use the cell average values to visualise the solution. This is in agreement with [45,5]. The solution structure observed on the 512×512 grid is comparable with the structure seen for the fifth order WENO method with Runge-Kutta time stepping presented in [45].

Rossmanith and Seal [38] used 5×5 points per grid cell to visualise the numerical approximations. Their fifth order accurate discontinuous Galerkin method uses 15 degrees of freedom per grid cell. Our two-dimensional third order accurate Active Flux method counts four degrees of freedom per grid cell as point values along the grid cell boundary are used by several grid cells. We may therefore compare the solution structure of the discontinuous Galerkin method with a more resolved Active Flux method. While the higher order polynomial reconstruction used in the discontinuous Galerkin method provides more structure within a grid cells, the Active Flux method with comparable number of degrees of freedom seems to lead to a comparable resolution of the filament structure. In Fig. 12 we present the evolution in time of relative deviations of the L^2-norm, total energy and entropy.

We conducted convergence studies for both the unlimited and limited method by comparing computations on sequences of grids. The results are given in Table 1 and confirm third order accuracy for both methods. The limited solutions were approximated using CFL = 0.25 and the unlimited using CFL = 0.5.

To demonstrate the effect and necessity of the positivity-preserving flux-limiter, we present in Fig. 11 enlarged views of the cross-sections of the solution structure. The limited solution remains non-negative, while the unlimited solution might become negative. In [24], the authors point out that the non-preservation of positivity might, in particular in long time simulations, lead to the development of unphysical numerical oscillations.

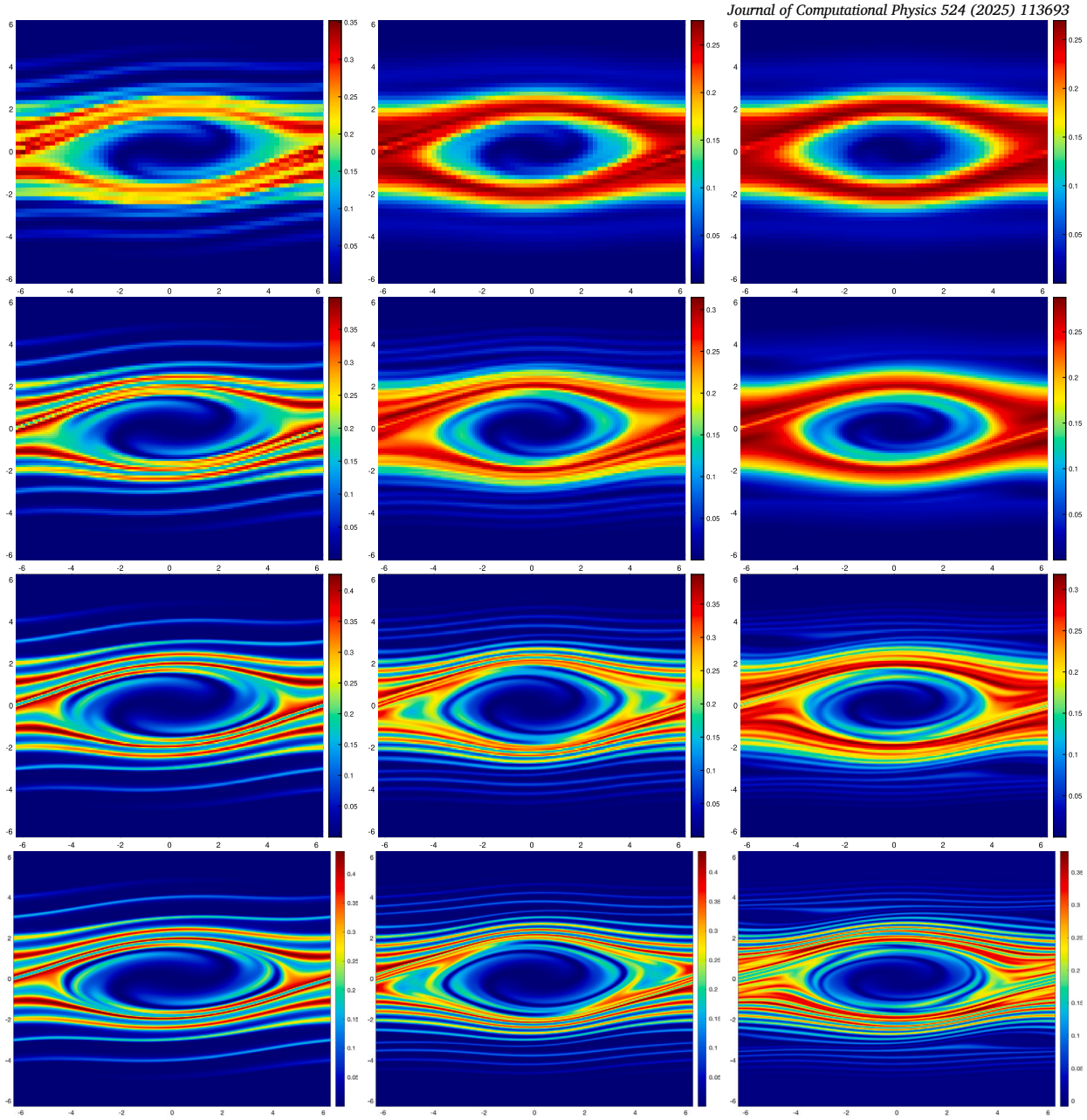

Fig. 9. Solutions of the two-stream instability problem computed with the positivity-preserving Active Flux method on grids with 64×64, 128×128, 256×256 and 512×512 cells (from top to bottom) at times $t = 15, 30, 45$ (from left to right).

4.4.2. Landau damping

In our second example we present results for weak Landau damping. We consider the following initial data

$$f(x, v, t = 0) = \frac{1}{\sqrt{2\pi}} (1 + \alpha \cos(kx)) \, e^{\frac{-v^2}{2}}, \tag{46}$$

with parameters $\alpha = 0.01$ and $k = 0.5$ and solve the Vlasov-Poisson system on the domain $(-2\pi, 2\pi) \times (-4.5, 4.5)$ with double periodic boundary conditions.

The example of weak Landau damping is especially interesting since one can investigate the decay of the L^2-norm of the electric field and compare it with the known linear decay rate given by $\gamma = -0.1533$. It is known that for periodic problems small initial perturbations lead to oscillations in the velocity distribution whose frequency grows in time and eventually leads to an under-resolved approximation and aliasing errors. When the charge density is computed from such an under-resolved Vlasov solution, the high frequencies are erroneously interpreted as low frequencies which leads to an inaccurate approximation of the charge density

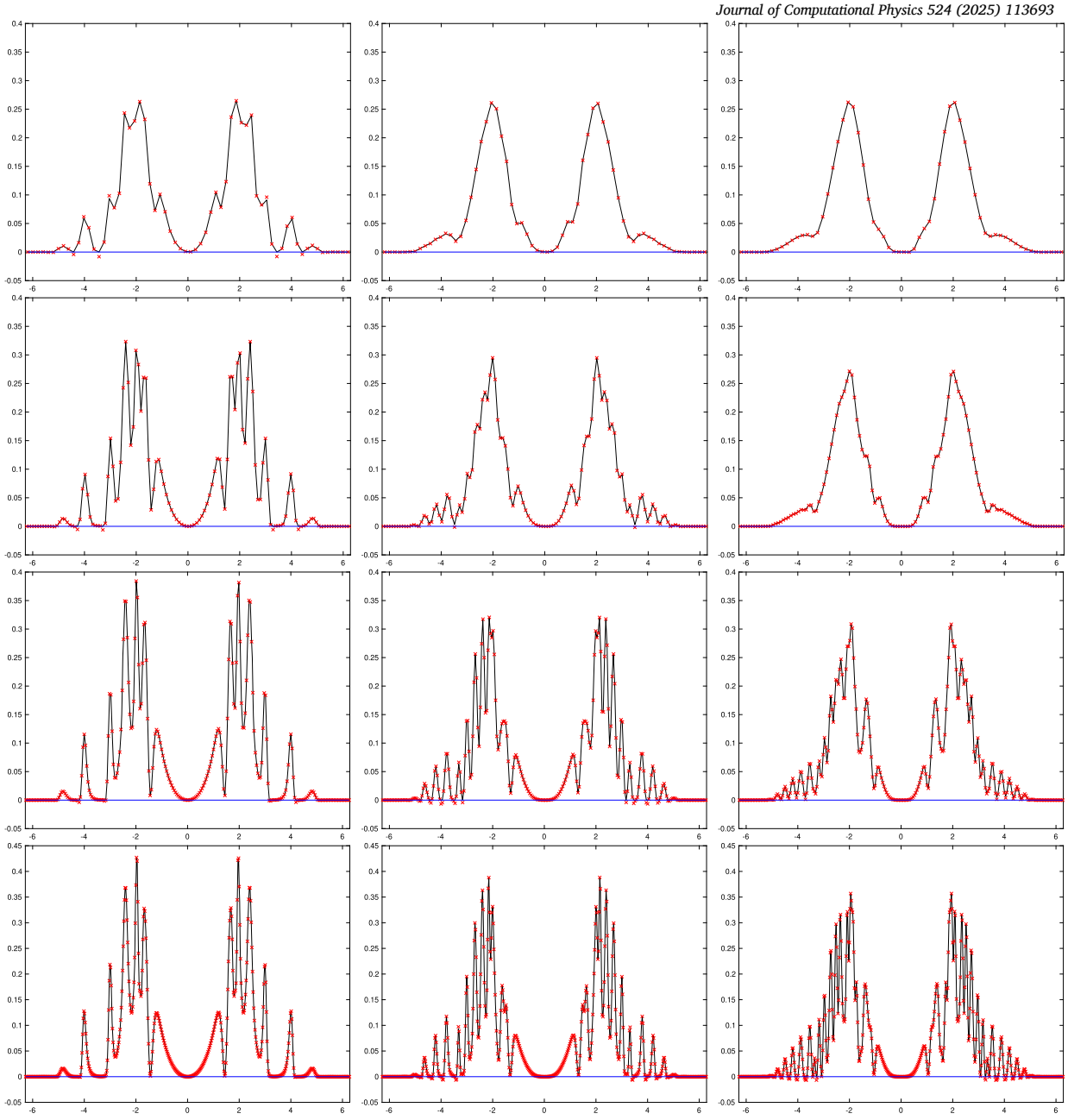

Fig. 10. Vertical cross sections at $x = 0$ of the numerical results from Fig. 9 for the two-stream instability problem at times $t = 15, 30, 45$ from left to right. The black solid line shows the limited non-negative solution. The red crosses show the corresponding unlimited solution. We use meshes with 64×64, 128×128, 256×256 and 512×512 cells from top to bottom.

and due to the coupling with the Poisson problem to an incorrect approximation of the electric energy. This so-called recurrence phenomenon was explained and studied for example in [5,32]. Since the Active Flux method is known to produce accurate results even on coarse grids, this is an interesting test problem for our method.

In Fig. 13, we present the decay of $\|E(\cdot,t)\|_{L^2}$ on meshes with 32×16, 32×32 and 32×64 grid cells using the Active Flux method with positivity-preserving limiter. These results can be compared with computations presented in [24, Fig. 3] where different methods were compared. On a grid with 32×32 grid cells our Active Flux method outperforms the positive and flux conservative (PFC) and the fourth order ENO method and compares well with the semi-Lagrangian method using cubic spline interpolation. A comparison with [24, Fig. 4] allows to compare the Active Flux method on these three different grids with the PFC method.

In order to compare our results with computational results shown in [38], we also computed the weak Landau damping problem on the domain $(-2\pi, 2\pi) \times (-2\pi, 2\pi)$ using more refined grids with 64×128, 128×256 and 256×512 cells. The results are shown

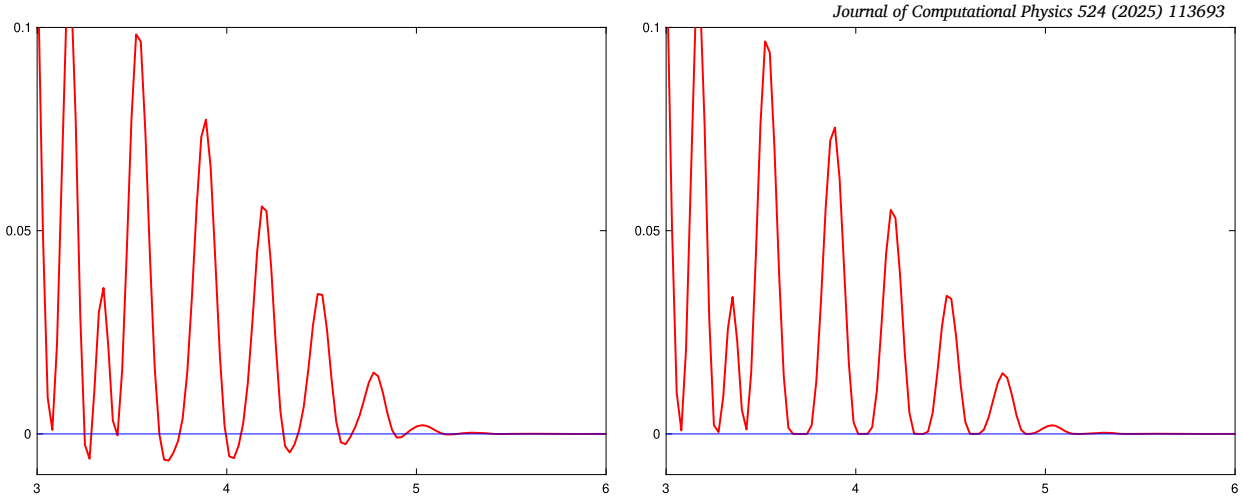

Fig. 11. Enlarged sections of the vertical cross-sections at $x = 0$ of the two-stream instability problem. Left: unlimited solution, right: limited solution.

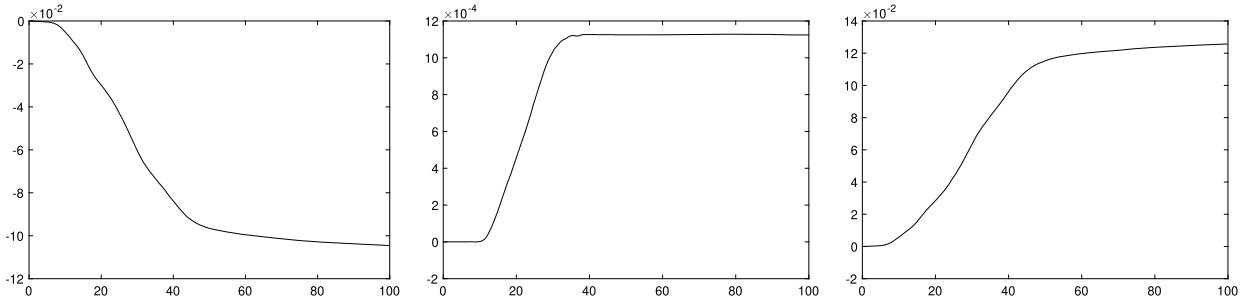

Fig. 12. Deviations of conserved quantities for the two-stream instability problem on a 256×256 grid. From left to right L^2-norm, total energy and entropy.

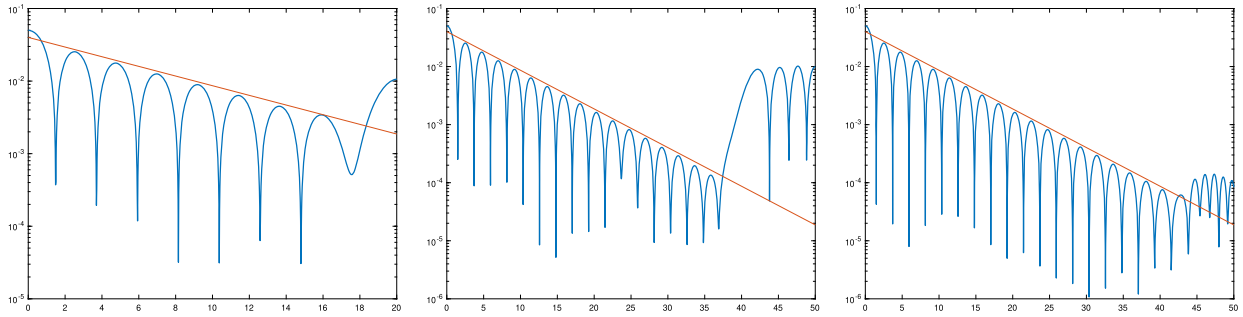

Fig. 13. $\|E\|_{L^2}$ for the weak Landau damping on grids with 32×16, 32×32 and 32×64 grid cells (from left to right). The orange line represents the theoretically predicted decay rate.

in Fig. 14. We obtain accurate results for $t \in [0, 60]$, i.e. the time interval used in [38, Fig. 8]. Here we also show the L^2-norm of the electric energy up to $t = 100$ to also show the onset of the recurrence phenomenon. Again, in Fig. 15 we present the evolution of relative deviations of the L^2-norm, total energy and entropy in time computed on a grid with 256×256 cells. For the weak Landau damping problem we did not observe a need for using the positivity-preserving flux limiter. The computational results shown in Fig. 14 and 15 have therefore been computed with the unlimited version of our Active Flux method using time steps according to $CFL \leq 0.75$. In fact, as long as no negative cell averages arise, the limited and unlimited methods coincide.

4.4.3. A multi-vortex two-stream instability

Next, we study the performance of our method for the multi-vortex two-stream instability, which was also considered in [10,16, 42,35]. We use the initial data

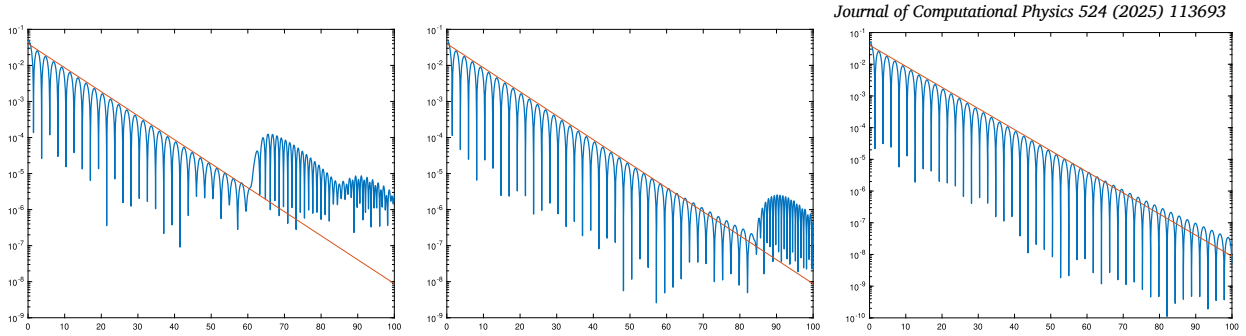

Fig. 14. $\|E\|_{L^2}$ for the weak Landau damping on grids with 64×128, 128×256 and 256×512 cells (from left to right). Again, the orange line represents the theoretically predicted decay rate.

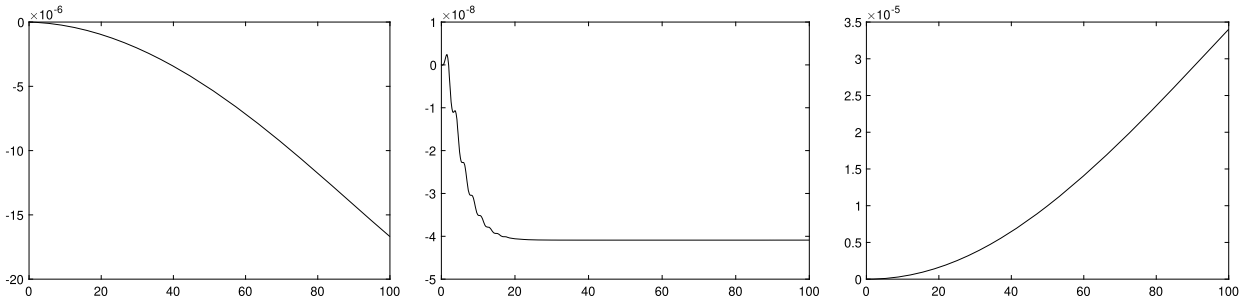

Fig. 15. Deviations of conserved quantities for the weak Landau problem on a 256×256 grid. From left to right L^2, total energy and entropy.

$$f(x,v,t=0)=\frac{1}{2v_{th}\sqrt{2\pi}}\left[\exp\left(-\frac{(v-u)^2}{2v_{th}^2}\right)+\exp\left(-\frac{(v+u)^2}{2v_{th}^2}\right)\right]\left(1+\alpha\hat{X}\right),$$

with $u=0.99$, $v_{th}=0.3$, $\alpha=0.05$, $v_{max}=5$ and $x\in[0,26\pi]$. In our description $\hat{X}\in(0,1)$ is a random perturbation added to the initial data. We consider calculations on grids with 128×128, 256×256 and 512×512 cells.

Caused by the initial perturbation, vortices start to form after some time. Independent on the grid resolution we observe the formation of 8-9 vortices on the considered domain. At later times the vortices start to merge. In the beginning the merging of vortices happens relatively quickly but slows down once there are only few vortices left.

In Fig. 16, we present the solution on the 512×512 grid and in Fig. 17 on the $128.\times128$ grid, in both cases at times $t=30,50,70,100,200,400$. All calculations have been performed using the positivity-preserving flux limiter. Additionally, in Fig. 18, we present the conservation of the L^2-norm, the electric energy and total energy.

4.4.4. The bump-on-tail instability

Finally, we consider another classical benchmark problem for Vlasov solvers which has been studied in many publications [36, 18,16,17]. For our simulations we used the initial data from [39,33] given by

$$f_0(x,v)=\tilde{f}(v)[1+\alpha\cos(kx)],\qquad (x,v)\in[0,L]\times[-v_{max},v_{max}] \tag{47}$$

with

$$\tilde{f}(v)=\frac{n_p}{\sqrt{2\pi}}\exp\left(\frac{-v^2}{2}\right)+\frac{n_b}{\sqrt{2\pi}}\exp\left(\frac{-|v-u|^2}{2v_t^2}\right). \tag{48}$$

We set $\alpha=0.04$ $k=0.3$, $n_p=0.9$, $n_b=0.2$, $u=4.5$, $v_t=0.5$, $L=20\pi$ and $v_{max}=9$. Furthermore, we consider a grid with $N_x=N_v=128$ cells and use the positivity-preserving flux-limiter. With these initial values three vortices form, which can be seen in Fig. 19. Additionally, we show plots of the spatially integrated distribution function at various times in Fig. 21.

Again, we are interested in the preservation of electric energy, L^2-norm and the total energy. In Fig. 20 we present the time evolution of these quantities. For the electrical energy, it can be seen that we first reach the maximum at $t\approx20$ followed by oscillations with decreasing amplitude in time until $t\approx300$ from then on the amplitude stays almost constant. This behaviour is in accordance with other results. For the L^2-norm we see a decrease which is comparable to what is observed for Lagrangian methods. The total energy is not preserved. This could be due to the fact that preserving both positivity and total energy is a difficult task, as mentioned in [16].

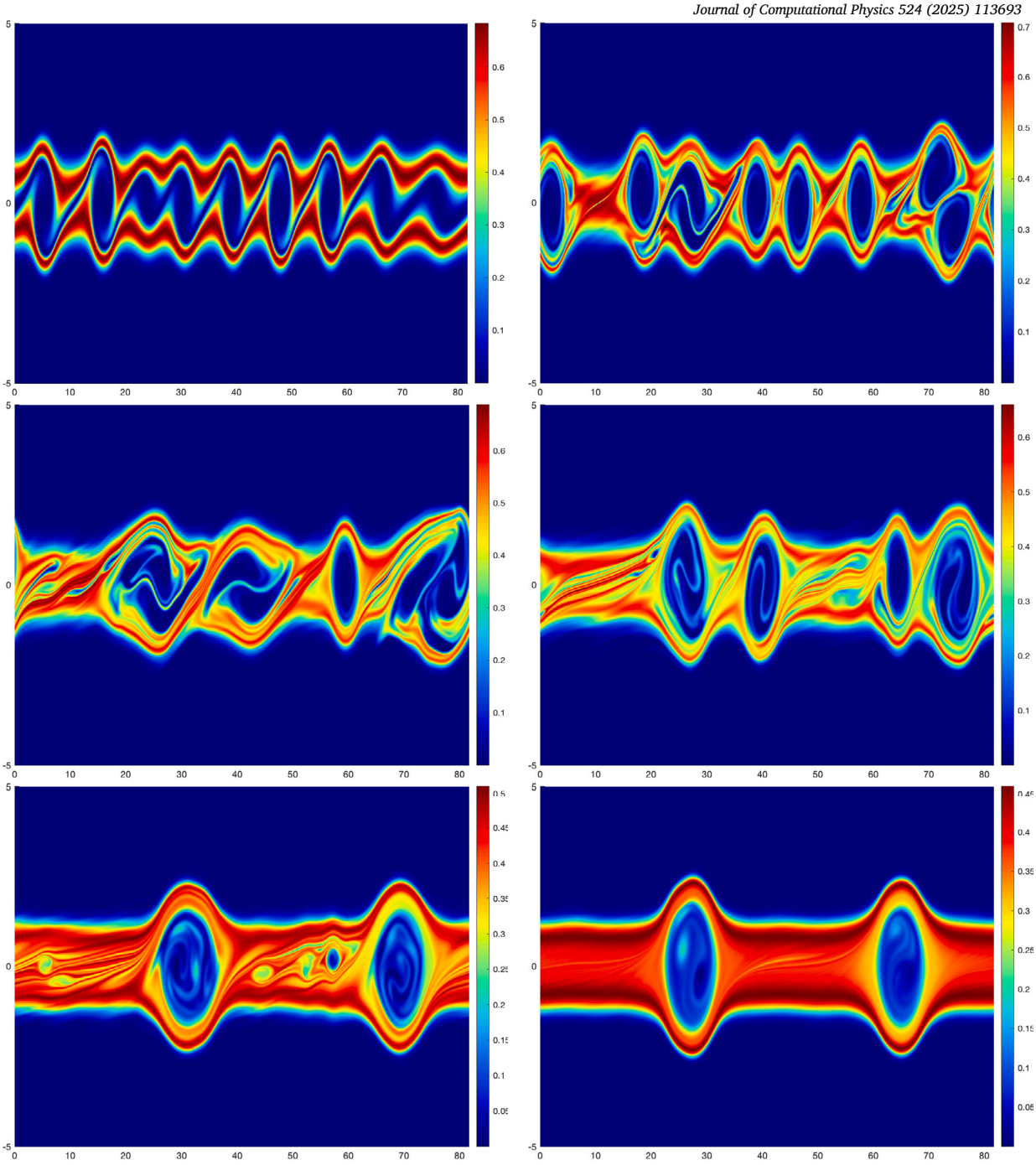

Fig. 16. Solutions to the multi-vortex two-stream instability at times $t = 30, 50, 70, 100, 200, 400$ from left to right and top to bottom with a resolution of $N_x = N_v = 512$.

5. Conclusions

In this work we presented an Active Flux method for the Vlasov-Poisson system in the $1 + 1$-dimensional case. Before we discussed this method, we introduced a positivity-preserving flux limiter for advective transport in a divergence-free velocity field. This limiting strategy relies on a bound-preserving property of the *Lax-Friedrichs* method. It does not affect the order of accuracy of the Active Flux method and is easy to implement. However, the preservation of positivity can only be guaranteed for a reduced CFL number. Afterwards we described in detail an Active Flux method for the Vlasov-Poisson system. Due to the additional point values located on the boundaries of the cells, we were able to develop a simple and efficient third order accurate positivity-preserving method that

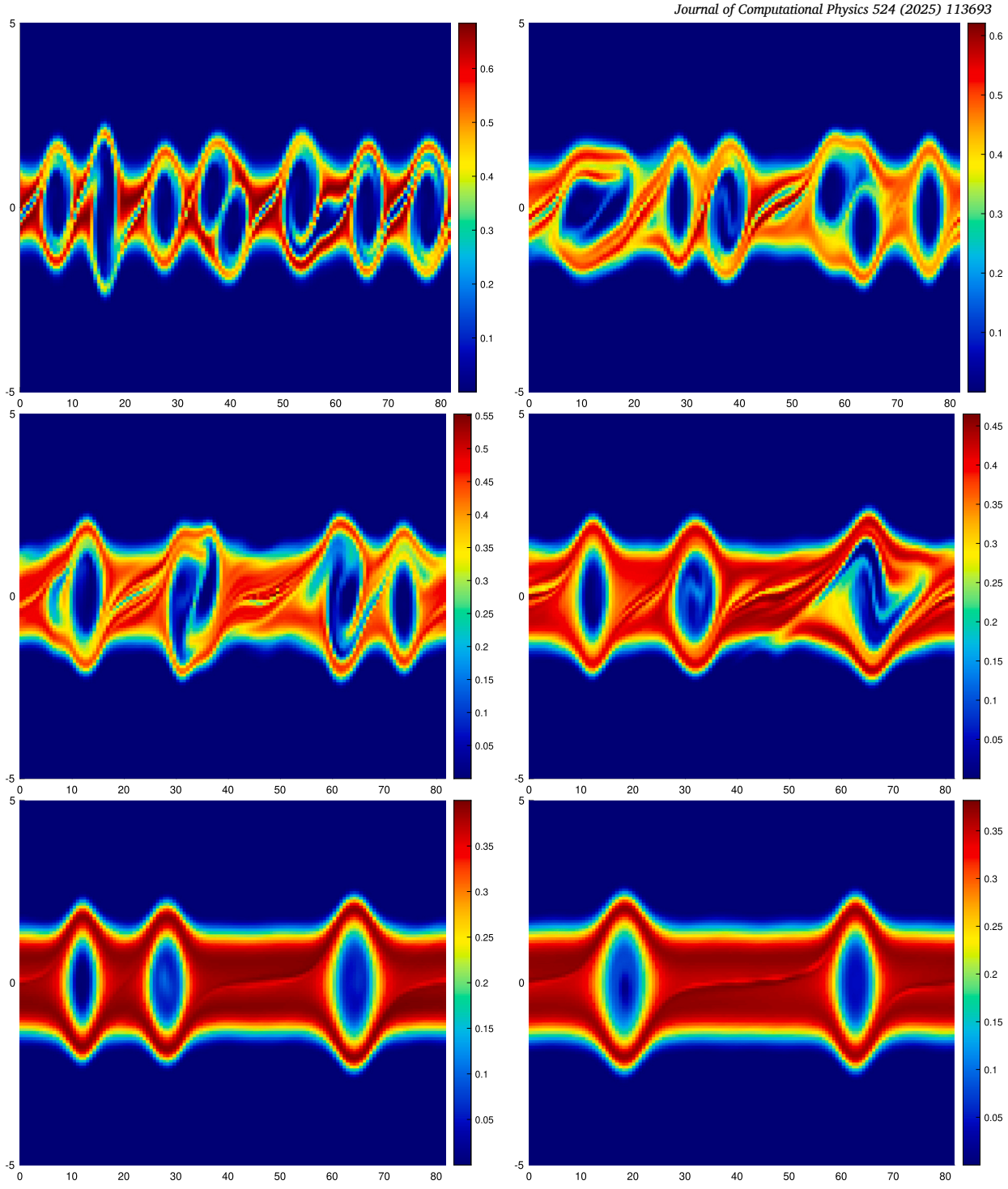

Fig. 17. Solutions to the multi-vortex two-stream instability at times $t = 30, 50, 70, 100, 200, 400$ from left to right and top to bottom with a resolution of $N_x = N_v = 128$.

requires only one solution of the Poisson problem and one solution of the Vlasov equation during each time step. We tested our method on classical tests for the Vlasov-Poisson problem.

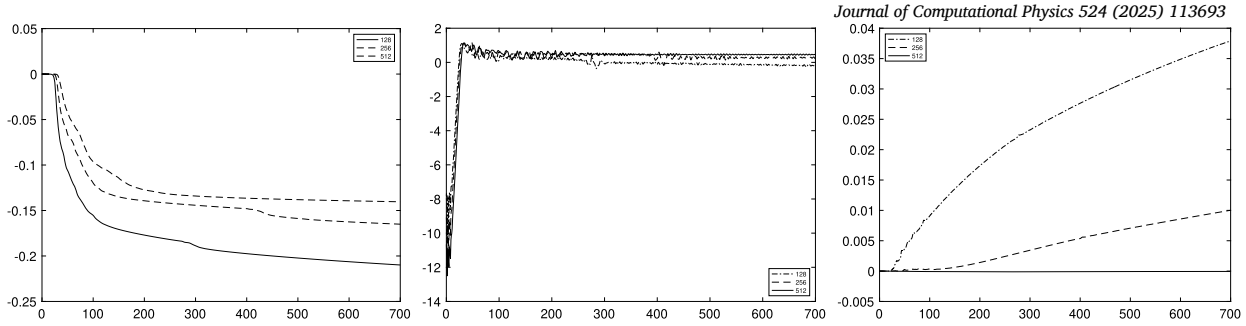

Fig. 18. Normalized deviation of L^2-norm (left) and total energy (right) as a function of time as well as time evolution of potential energy in semi-log scale (middle) on grids with 128×128, 256×256 and 512×512 cells for the multi-vortex two-stream instability.

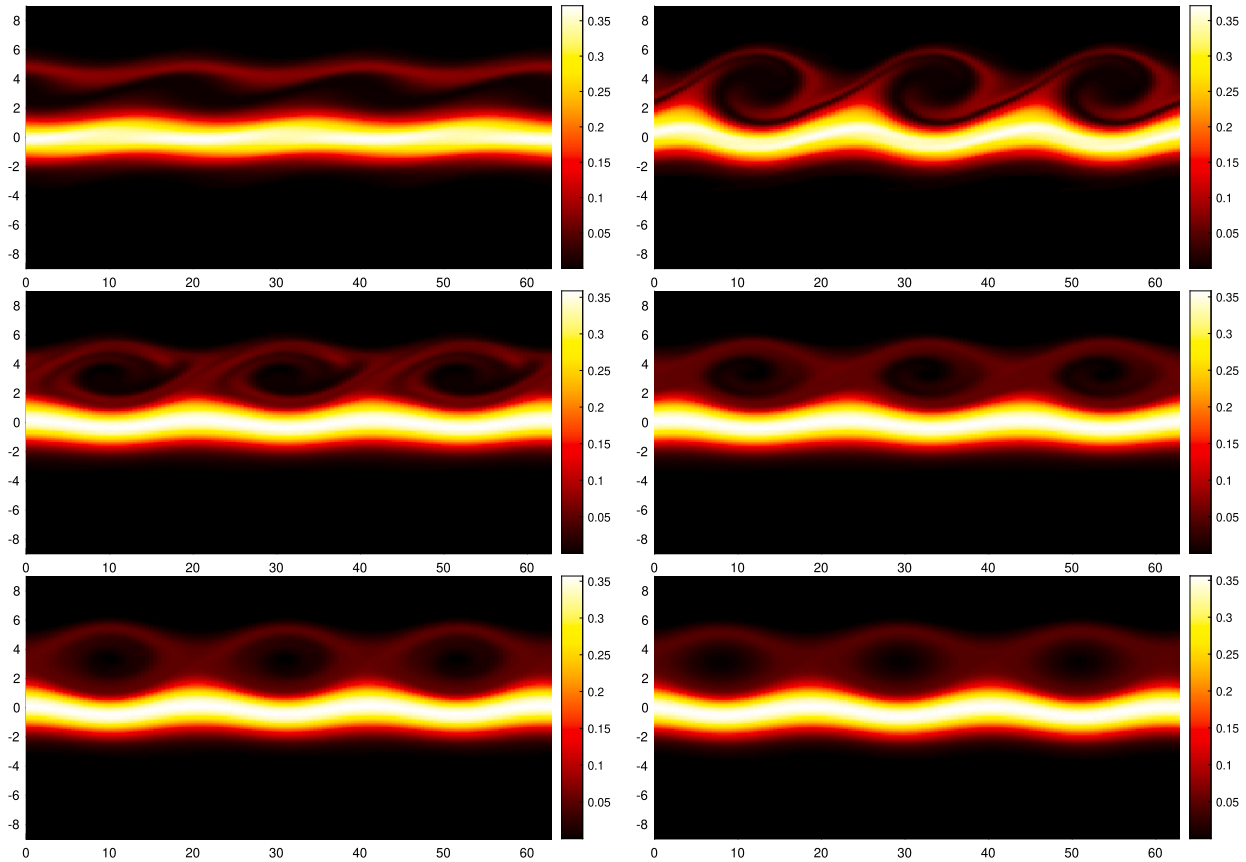

Fig. 19. Solutions to the Bump on Tail instability at times $t = 10, 20, 50, 100, 200, 400$ from left to right and top to bottom with a resolution of $N_x = N_v = 128$.

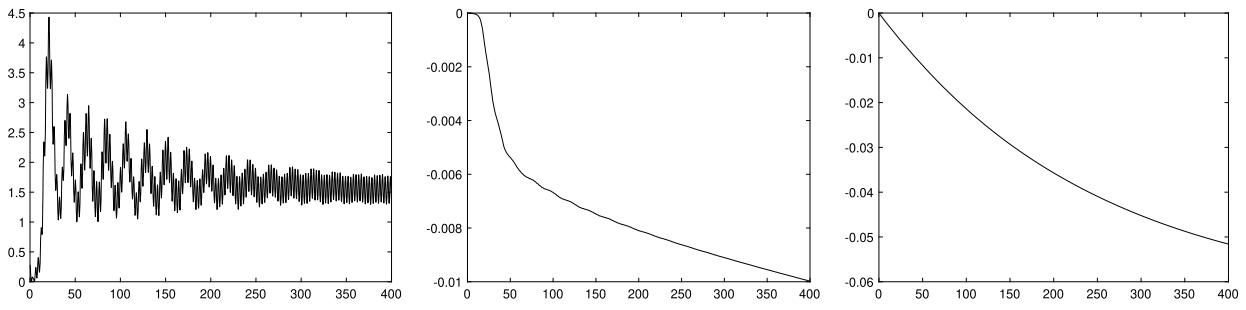

Fig. 20. Time evolution of the electric energy (left), L^2-norm (middle) and total energy (right) of the Bump on Tail instability on a 128×128 grid.

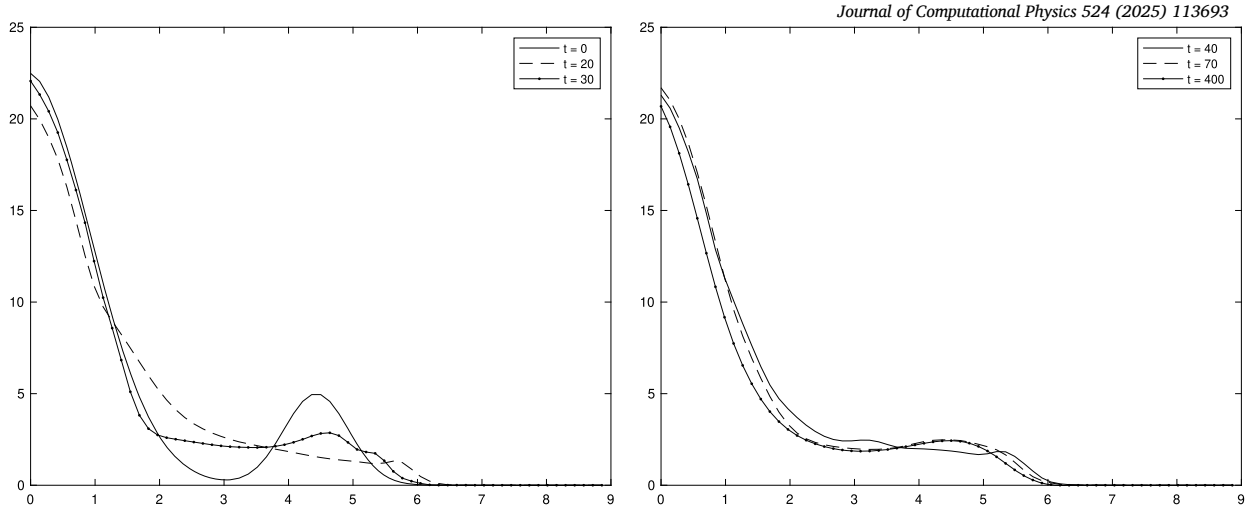

Fig. 21. Spatially integrated distribution function of the Bump on Tail instability on a 128×128 grid at times $t = 0, 20, 30, 40, 70, 400$.

CRediT authorship contribution statement

Yanick Kiechle: Writing – original draft, Software, Investigation. **Erik Chudzik:** Software, Investigation. **Christiane Helzel:** Writing – review & editing, Investigation, Conceptualization.

Declaration of competing interest

The authors declare the following financial interests/personal relationships which may be considered as potential competing interests: Christiane Helzel reports financial support was provided by Deutsche Forschungsgemeinschaft. If there are other authors, they declare that they have no known competing financial interests or personal relationships that could have appeared to influence the work reported in this paper.

Acknowledgements

Funded by the Deutsche Forschungsgemeinschaft (DFG, German Research Foundation) through FOR 5409 Structure-preserving Numerical Methods for Bulk and Interface Coupling of Heterogeneous Models, within the project *An Active Flux Method for the Vlasov-Maxwell System* 463312734.

We thank our project partners, in particular Rainer Grauer and Gudrun Grünwald from Bochum, for fruitful discussions.

Data availability

No data was used for the research described in the article.

References

[1] R. Abgrall, W. Barsukow, Extensions of active flux to arbitrary order of accuracy, arXiv:2208.14476, 2022.
[2] R. Abgrall, W. Barsukow, C. Klingenberg, The active flux method for the Euler equations on Cartesian grids, arXiv:2310.00683v1, 2023.
[3] R. Abgrall, M. Jiao, Y. Liu, K. Wu, Bound preserving point-average-moment polynomial-interpreted (PAMPA) scheme: one-dimensional case, arXiv:2410.14292, 2024.
[4] F. Allmann-Rahn, S. Lautenbach, R. Grauer, An energy conserving Vlasov solver that tolerates coarse velocity space resolution: simulation of MMS reconnection events, J. Geophys. Res. Space Phys. 127 (2) (2022), https://doi.org/10.1029/2021JA029976.
[5] J. Banks, J. Hittinger, A new class of nonlinear finite-volume methods for Vlasov simulation, IEEE Trans. Plasma Sci. 38 (9) (2010) 2198–2207.
[6] W. Barsukow, The active flux scheme for nonlinear problems, J. Sci. Comput. 86 (3) (2021) 1–34.
[7] W. Barsukow, J. Hohm, C. Klingenberg, P. Roe, The active flux scheme on Cartesian grids and its low Mach number limit, J. Sci. Comput. 81 (2019) 594–622.
[8] R. Belaouar, N. Crouseilles, P. Degond, E. Sonnendrücker, An asymptotically stable semi-Lagrangian scheme in the quasi-neutral limit, J. Sci. Comput. 41 (3) (2009) 341–365.
[9] N. Besse, E. Sonnendrücker, Semi-Lagrangian schemes for the Vlasov equation on an unstructured mesh of phase space, J. Comput. Phys. 191 (2) (2003) 341–376.
[10] X. Cai, W. Guo, J.-M. Qiu, A high order semi-Lagrangian discontinuous Galerkin method for Vlasov–Poisson simulations without operator splitting, J. Comput. Phys. 354 (2018) 529–551.
[11] D. Calhoun, E. Chudzik, C. Helzel, The Cartesian grid active flux method with adaptive mesh refinement, J. Sci. Comput. 94 (2023).
[12] C. Cheng, G. Knorr, The integration of the Vlasov equation in configuration space, J. Comput. Phys. 22 (3) (1976) 330–351.
[13] E. Chudzik, C. Helzel, D. Kerkmann, The Cartesian grid active flux method: linear stability and bound preserving limiting, Appl. Math. Comput. 393 (2021) 125501.
[14] E. Chudzik, C. Helzel, M. Lukáčová-Medvid'ová, Active flux methods for hyperbolic systems using the method of bicharacteristics, J. Sci. Comput. 99 (1) (2024) 16.

[15] N. Crouseilles, P. Glanc, S.A. Hirstoaga, E. Madaule, M. Mehrenberger, J. Pétri, A new fully two-dimensional conservative semi-Lagrangian method: applications on polar grids, from diocotron instability to ITG turbulence, Eur. Phys. J. D 68 (9) (2014) 252.
[16] N. Crouseilles, M. Mehrenberger, E. Sonnendrücker, Conservative semi-Lagrangian schemes for Vlasov equations, J. Comput. Phys. 229 (6) (2010) 1927–1953.
[17] N. Crouseilles, M. Mehrenberger, F. Vecil, Discontinuous Galerkin semi-Lagrangian method for Vlasov-Poisson, ESAIM Proc. 32 (2011) 211–230.
[18] N. Crouseilles, T. Respaud, E. Sonnendrücker, A forward semi-Lagrangian method for the numerical solution of the Vlasov equation, Comput. Phys. Commun. 180 (10) (2009) 1730–1745.
[19] T. Eymann, P. Roe, Active flux schemes for systems, AIAA 2011-3840, 2011.
[20] T. Eymann, P. Roe, Multidimensional active flux schemes, AIAA Conference Paper, 2013.
[21] D. Fan, P. Roe, Investigations of a new scheme for wave propagation, in: AIAA Aviation Forum, 2015.
[22] F. Filbet, E. Sonnendrücker, Numerical methods for the Vlasov equation, in: F. Brezzi, A. Buffa, S. Corsaro, A. Murli (Eds.), Numerical Mathematics and Advanced Applications., Springer, Milan, 2003, pp. 459–468.
[23] F. Filbet, E. Sonnendrücker, Comparison of Eulerian Vlasov solvers, Comput. Phys. Commun. 150 (3) (2003) 247–266.
[24] F. Filbet, E. Sonnendrücker, P. Bertrand, Conservative numerical schemes for the Vlasov equation, J. Comput. Phys. 172 (1) (2001) 166–187, https://doi.org/10.1006/jcph.2001.6818.
[25] F. Filbet, T. Xiong, Conservative discontinuous Galerkin/Hermite spectral method for the Vlasov–Poisson system, Commun. Appl. Math. Comput. 4 (1) (2022) 34–59, https://doi.org/10.1007/s42967-020-00089-z.
[26] C. Helzel, D. Kerkmann, L. Scandurra, A new ADER method inspired by the active flux method, J. Sci. Comput. 80 (2019) 1463–1497.
[27] R. Hockney, J. Eastwood, Computer Simulation Using Particles, Institute of Physics Publishing, 1988.
[28] X. Hu, N. Adams, C.-W. Shu, Positivity-preserving method for high-order conservative schemes solving compressible Euler equations, J. Comput. Phys. 242 (2013) 169–180, https://doi.org/10.1016/j.jcp.2013.01.024.
[29] Y.-F. Kiechle, E. Chudzik, C. Helzel, An active flux method for the Vlasov-Poisson system, in: E. Franck, J. Fuhrmann, V. Michel-Dansac, L. Navoret (Eds.), Finite Volumes for Complex Applications X—Volume 2, Hyperbolic and Related Problems, Springer Nature, Switzerland, 2023, pp. 93–101.
[30] R. LeVeque, High-resolution conservative algorithms for advection in incompressible flow, J. Numer. Anal. 33 (2) (1996) 627–665, https://doi.org/10.1137/0733033.
[31] M. Mehrenberger, L.S. Mendoza, C. Prouveur, E. Sonnendrücker, Solving the guiding-center model on a regular hexagonal mesh, ESAIM Proc. Surv. 53 (2016) 149–176.
[32] M. Mehrenberger, L. Navoret, N. Pham, Recurrence phenomenon for Vlasov-Poisson simulations on regular finite element mesh, Commun. Comput. Phys. 28 (3) (2020) 877–901.
[33] T. Nakamura, T. Yabe, Cubic interpolated propagation scheme for solving the hyper-dimensional Vlasov—Poisson equation in phase space, Comput. Phys. Commun. 120 (2) (1999) 122–154, https://doi.org/10.1016/S0010-4655(99)00247-7.
[34] J.-M. Qiu, A. Christlieb, A conservative high order semi-Lagrangian WENO method for the Vlasov equation, J. Comput. Phys. 229 (4) (2010) 1130–1149.
[35] J.-M. Qiu, C.-W. Shu, Positivity preserving semi-Lagrangian discontinuous Galerkin formulation: theoretical analysis and application to the Vlasov–Poisson system, J. Comput. Phys. 230 (23) (2011) 8386–8409.
[36] T. Respaud, E. Sonnendrücker, Analysis of a new class of forward semi-Lagrangian schemes for the 1D Vlasov Poisson equations, Numer. Math. 118 (2) (2011) 329–366.
[37] P. Roe, Designing CFD methods for bandwidth - a physical approach, Comput. Fluids 214 (2021) 104774, https://doi.org/10.1016/j.compfluid.2020.104774.
[38] J. Rossmanith, D. Seal, A positivity-preserving high-order semi-Lagrangian discontinuous Galerkin scheme for the Vlasov-Poisson equations, J. Comput. Phys. 230 (2011) 6203–6232, https://doi.org/10.1016/j.jcp.2011.04.018.
[39] M.M. Shoucri, Nonlinear evolution of the bump-on-tail instability, Phys. Fluids 22 (10) (1979) 2038–2039.
[40] E. Sonnendrücker, J. Roche, P. Bertrand, A. Ghizzo, The semi-Lagrangian method for the numerical resolution of the Vlasov equation, J. Comput. Phys. 149 (2) (1999) 201–220, https://doi.org/10.1006/jcph.1998.6148.
[41] E. Sonnendrücker, J. Roche, P. Bertrand, A. Ghizzo, The semi-Lagrangian method for the numerical resolution of the Vlasov equation, J. Comput. Phys. 149 (2) (1999) 201–220.
[42] T. Umeda, A conservative and non-oscillatory scheme for Vlasov code simulations, Earth Planets Space 60 (7) (2008) 773–779.
[43] B. van Leer, Towards the ultimate conservative difference scheme. IV. A new approach to numerical convection, J. Comput. Phys. 23 (1977) 276–299, https://doi.org/10.1016/0021-9991(77)90095-X.
[44] T. Xiong, J.-M. Qiu, Z. Xu, A. Christlieb, High order maximum principle preserving semi-Lagrangian finite difference WENO schemes for the Vlasov equation, J. Comput. Phys. 273 (2014) 618–639, https://doi.org/10.1137/140965326.
[45] X. Zhang, C.-W. Shu, On maximum-principle-satisfying high order schemes for scalar conservation laws, J. Comput. Phys. 229 (2010) 3091–3120, https://doi.org/10.1016/j.jcp.2009.12.030.
[46] X. Zhang, C.-W. Shu, On positivity-preserving high order discontinuous Galerkin schemes for compressible Euler equations on rectangular meshes, J. Comput. Phys. 229 (23) (2010) 8918–8934, https://doi.org/10.1016/j.jcp.2010.08.016.
[47] X. Zhang, C.-W. Shu, Maximum-principle-satisfying and positivity-preserving high-order schemes for conservation laws: survey and new developments, Proc. R. Soc. A 476 (2011) 2752–2776, https://doi.org/10.1098/rspa.2011.0153.